Wavelengths and Energy Levels of Neutral Manganese (Mn I) Determined Using High-Resolution Fourier Transform and Grating Spectroscopy

CHRISTIAN P. CLEAR , GILLIAN NAVE , RICHARD BLACKWELL-WHITEHEAD, MARIA TERESA BELMONTE , STEPHEN INGRAM, AND JULIET C. PICKERING

¹Physics Department, Imperial College London, London, SW7 2AZ, UK
 ²National Institute of Standards and Technology, Gaithersburg, MD, 20889-8422, USA
 ³Universidad de Valladolid, Departamento de Física Teórica, Atómica y Óptica, P. de Belén, 7, Valladolid 47011, Spain

ABSTRACT

An extensive analysis of the spectrum of neutral manganese has been performed using spectra of manganese-neon and manganese-argon hollow cathode discharges measured using high resolution Fourier transform (FT) and grating spectroscopy over the range 151 - 5112 nm (1956 - 65876 cm⁻¹). Wavelengths for 10426 spectral lines were extracted from the FT spectra, with uncertainties at least an order-of-magnitude lower than previous measurements. Wavelengths for 13397 lines from new grating spectra were determined for spectral regions beyond the FT spectra range or to provide wavelengths for weak transitions not observed in FT spectra. To aid in level identification, selected, previously published grating lines were included in the energy level optimisation, but no levels in this work relied solely on previously published wavelengths. In total, 24237 lines were included in the final spectral linelist, and these were used to identify 2186 Mn I transitions. These classified spectral lines were then used to optimise the values of 384 previously published energy levels of Mn I, with typical uncertainties of a few 10⁻³ cm⁻¹, again typically an order-of-magnitude improvement in accuracy. Our study then expanded the known energy level structure of Mn I through the establishment of 18 new energy levels, reported here for the first time. In total, 2187 lines and 402 energy levels of Mn I have been determined as a result of our work, marking a substantial advance in the precision of Mn I atomic data which will enable far more accurate analyses of Mn I lines in astrophysical spectra.

Keywords: Atomic spectroscopy (2099); Line positions (2085); Spectroscopy (1558); Laboratory astrophysics (2004); Spectral line identification (2073); Experimental techniques (2078); Spectral line lists (2082); Stellar atmospheric opacity (1585); Stellar spectral lines (1630); Atomic data benchmarking (2064)

1. INTRODUCTION

The rapid advancement of high-resolution spectrographs on both ground-based and space-borne telescopes, such as HST-STIS, VLT-UVES, and JWST, has dramatically expanded our ability to observe astrophysical spectra in unprecedented detail. However, the analysis of these spectra continues to be hindered by a lack of sufficiently accurate and comprehensive laboratory data, particularly among the iron-group elements. These elements, with their complex electron configurations and high relative abundances, give rise to dense forests of spectral lines that are prominent across the

Corresponding author: Christian Clear christian.clear@imperial.ac.uk

ultraviolet (UV) to infrared (IR) regions, playing a critical role in shaping the absorption and emission features of many astrophysical environments. In response, collaborative efforts led by Imperial College London (ICL) and the National Institute for Standards and Technology (NIST) have focussed on improving wavelengths and energy levels for neutral species through high-resolution Fourier transform (FT) and grating spectroscopy. These measurements are essential for interpreting stellar spectra, especially in cool stars and early-type stellar atmospheres, where neutral atomic species dominate spectral opacities.

Modern stellar astrophysical models are now being analysed in three dimensions and are taking into account departures from local thermodynamic equilibrium. Non-local thermodynamic equilibrium (NLTE) conditions arise when atomic level populations are determined by radiation fields and non-local processes, rather than being governed solely by the local plasma temperature and density. Neutral manganese (Mn I) is particularly sensitive to NLTE effects, more so than Mn II (Bergemann, M. et al. 2019), where effects such as overionisation, driven by ultraviolet radiation, can significantly weaken spectral lines, leading to systematic underestimation of Mn abundances if LTE is assumed. Modern stellar models require large amounts of atomic data to enable reliable NLTE modelling and improve abundance determinations across a wide range of stellar environments, underscoring the urgent need for high-precision atomic data for Mn I, particularly accurate energy levels and transition wavelengths.

1.1. Previous Measurements of Mn I

Previous measurements of the spectrum of Mn I fall into two main groups. The older group consists of low resolution spectral line measurements obtained from broad wavelength range spectra, conducted using grating and prism spectrometers. The majority of energy levels derived from these older line measurements have uncertainties of $\sim 0.1~{\rm cm}^{-1}$. These data now fall far below the accuracy requirements of modern, high resolution astrophysical spectroscopy. The more recent group of measurements have been made using laser spectroscopy and interferometric techniques, typically with higher resolutions $(0.05 \text{ cm}^{-1} \text{ to } 0.0001 \text{ cm}^{-1})$. However, these newer measurements have been for specific, limited sets of lines, accounting for a small fraction of the total observable transitions in the spectrum of Mn I and are primarily concerned with studies of hyperfine structure (HFS) or the determination of atomic energy level lifetimes.

The first large-scale study of the spectrum and energy level system of Mn I was performed by M. A. Catalán (1923) using prism and grating spectroscopy of flamearc, arc and spark sources at ICL whilst a research student under Prof A Fowler. Catalán determined wavelengths for 169 Mn I lines in the spectral range 257 - $1760 \text{ nm} (5677-38815 \text{ cm}^{-1}), \text{ using these lines to iden-}$ tify 32 low-lying energy levels. Catalán was the first to observe and comment on the appearance of repeated patterns of transitions in the spectrum of manganese, which he called "multiplets", which led to the general recognition of the multiplet structure of other complex spectra. In 1926, absorption measurements in the region $187 - 1761 \text{ nm} (5679 - 53342 \text{ cm}^{-1}) \text{ by J. C. McLennan}$ & A. McLay (1926) extended the work of Catalán, increasing the number of known energy levels to 90 and the number of identified lines to 257.

In 1945 Charlotte Moore produced a "Multiplet Table of Astrophysical Interest" (C. E. Moore 1945) as part of her comprehensive review of atomic energy levels. Moore's comments on the lack of available data for Mn I prompted Catalán to set his student Olga Garcia-Riquelme the task of reassessing the data on Mn I. In 1949, O. García-Riquelme (1949) compiled all known wavelengths, line intensities and energy level values of Mn I from 15 different authors and analysed these to find 58 new energy levels. Fifteen years later, M. A. Catalán et al. (1964) published the last major work (note that this paper was finished after Catalán's death in 1957) on Mn I wavelengths and energy levels. They reviewed the quality of all available Mn I data (including unpublished work by T. Dunham Jr.) and re-analysed the data to identify further Mn I transitions, bringing the total number of line wavelengths to 2030 across the wavelength range 178 - 1761 nm $(5677 - 56011 \text{ cm}^{-1})$ and resulting in determination of 404 energy levels in total.

The most recent published compilation of Mn I energy levels is the 1985 work by J. Sugar & C. Corliss (1985), referred to from now on as S&C. The majority of level values in the S&C compilation are taken directly from M. A. Catalán et al. (1964). As no energy level uncertainties were given by Catalán et al, S&C estimated these from differences between Ritz and observed wavelengths to be ± 0.1 cm⁻¹. S&C also included a small number of high lying $3d^64s(^7S)np$ energy levels, identified from low-resolution absorption spectra recorded by M. L. Ginter & C. M. Brown (1978), estimating their uncertainty to be ± 0.05 cm⁻¹. A more recent publication by A. G. Taklif (1990) identified 53 new Mn I lines in the IR between 0.82 and 1.97 μm (5068 - 11929 cm⁻¹), but using low-resolution grating spectra (resolution 0.008 nm), and no analysis to determine new energy levels was performed.

Although the range of the previously existing spectral data for Mn I extends from the vacuum UV (VUV) to the IR, the quality of the measurements varies immensely. Only approximately 5\% of the spectral lines in the visible have been measured with wavenumber uncertainty of ≤ 0.05 cm⁻¹ or better. Indeed, the majority of lines are only known to an uncertainty of 0.1 cm^{-1} or worse. The accuracies of these data now fall far short of the requirements of high-resolution astrophysical spectral analyses. Furthermore, with the exception of a small number of lines measured to obtain HFS splitting factors (e.g. R. Blackwell-Whitehead et al. (2005) and selected references therein), the majority of spectra in the literature have been measured at low resolutions, which are insufficient to resolve many of the complex features of the Mn I spectrum. With high resolution FT spectroscopy it is now possible to reduce the uncertainties of transition wavelengths and energy levels of Mn I by at least an order of magnitude.

This work addresses the critical need for Mn I atomic data. As a result of an extensive term analysis of Mn I, this paper presents new and improved energy level values and transition wavelengths for Mn I, which will be invaluable in the interpretation of stellar and laboratory spectra across a wide range of astrophysical and applied contexts.

2. EXPERIMENTAL DETAILS

The FT and grating spectra used in this work were previously employed in the energy level analysis of Mn II by F. S. Liggins et al. (2021), where full details of the spectral acquisition and calibration procedures are described in its Section 2. We provide a brief summary of these details in the following sections. These spectra provide a rich and well-characterised dataset that forms the foundation of the present term analysis of Mn I. For completeness, a brief summary of the relevant spectra and the resulting linelists is given in the following sections.

In addition, to support the identification and confirmation of several energy levels in Mn I, we incorporated the historical line list of M. A. Catalán et al. (1964). Due to the lower accuracy of this legacy dataset compared to the new FTS and grating data, Calatán's lines were used primarily to check level assignments where only a small number of FTS or grating lines were available. All energy levels given in this paper have at least one FTS or newly-measured grating line. A discussion of our uncertainty estimates for Catalán's lines is provided in Section 2.3.

2.1. Fourier Transform (FT) Spectroscopy

High-resolution FT spectra were recorded at ICL and NIST, covering a broad spectral range from the IR to the VUV. Measurements in the visible to VUV region $(24,005-58,990 \text{ cm}^{-1})$ were obtained using the ICL UVand VUV-FT spectrometers (A. P. Thorne et al. 1987; A. Thorne 1996), while IR spectra $(1.820-26.632 \text{ cm}^{-1})$ were recorded at NIST using the 2m FT spectrometer (G. Nave et al. 1997). Additional lines were extracted from high-current FT spectra recorded by R. Kling & U. Griesmann (2000), originally intended for measurements of Mn II transition probabilities. While selfabsorption affected stronger lines in these high-current spectra, weaker Mn I lines were present that were not observed in other spectra. A summary of the FTS spectra used in this work is given in Table 1.

Water-cooled hollow cathode lamps (HCLs) with argon or neon carrier gases served as the emission sources

for the spectra. To mitigate the brittleness of pure Mn, cathodes were fabricated from Mn–Cu (95:5) and Mn–Ni (88:12) alloys for the NIST and ICL spectra, respectively. The HCLs produced emission from Mn I, Mn II, neutral and singly ionised carrier gas lines (Ar or Ne), and impurity lines from the cathode alloy metals. Optimal operating conditions were 0.9 mbar of Ar or 3.4 mbar of Ne at 450 mA. Additional low-current runs at 200 mA, under the same pressures, were performed to assess self-absorption in strong metal lines. The resolution of the spectra ranged from 0.009 cm⁻¹ in the IR to 0.08 cm⁻¹ in the VUV.

Intensity calibration was achieved by recording the spectrum of a radiometrically calibrated standard lamp immediately before and after each HCL measurement. Comparison of the averaged standard lamp spectrum to the calibrated radiance of the standard lamp enabled determination of the average instrument response function over the measurement period. Relative line intensities were obtained by dividing observed intensities by the response function. A tungsten standard lamp calibrated by the National Physical Laboratory (NPL), UK, was used at ICL for calibration of spectra in the IR to visible regions. Another tungsten lamp, calibrated by Optronics Laboratories Inc., USA, was used for all the NIST spectra. Deuterium standard lamps with either silica or MgF₂ windows were used in the visible to UV and VUV regions at ICL, with calibrations performed by NPL and the Physikalisch-Technische Bundesanstalt (PTB), Germany, respectively.

All spectra were placed on a common relative intensity scale using strong metal lines in overlapping regions to determine scaling factors. The relative populations of energy levels and resulting line intensities depend on the carrier gas, current, and pressure of each HCL. The relative line intensities presented here are approximate and should not be used for precise calculations of level branching fractions or transition probabilities.

The wavenumber, integrated intensity, full width at half maximum (FWHM), and signal-to-noise ratio (S/N) were measured for each spectral line using the spectral analysis software Xgremlin (G. Nave et al. 2015). For lines without observed asymmetries, least-squares fits to Voigt profiles were performed. For asymmetric lines and those with significant HFS, centre-of-gravity (CoG) fits were used to determine the centroid wavenumber. CoG fits were used for the majority of lines in the FT spectra.

For certain critical transitions, such as resonance lines, key intercombination lines, or cases where line identifications were uncertain, a detailed HFS fit was required, especially when the measured wavenumber uncertainty was much higher than expected from the signal-to-noise

Table 1. FT spectra used in the Mn I analysis

Date/	Region used	Instrument	Filter	Detector	Resolution	Current	Pressure	Gas	$k_{ m eff}$ *	Note †
Serial no.	(cm^{-1})				(cm^{-1})	(A)	(Pa)		(10^{-7})	
2001 Jan 25 no. 2	1820 - 9550	NIST 2m	-	InSb	0.01	1.2	75	Ar	$3.2^* \pm 0.2$	maah
2001 Jan 26 no. 3	1820 - 9550	NIST 2m	-	InSb	0.01	1.5	250	Ne	$2.23^* \pm 0.17$	manh
2001 Jan 19 no. 4	4010 - 17490	NIST 2m	-	InSb	0.009	1.5	250	Ne	$2.50^* \pm 0.16$	mcnh
2001 Jan 22 no. 14	8520 - 24985	NIST 2m	-	Si	0.013	1.2	75	Ar	$2.55^* \pm 0.12$	meah
2001 Jan 16 no. 3	8443 - 25291	NIST 2m	-	Si	0.013	1.7	250	Ne	$2.31^* \pm 0.07$	menh
2001 Jan 16 no. 8	15 918 - 24 985	NIST 2m	CuSO_4	Si	0.02	1.0	80	Ar	$2.08 \pm\ 0.02$	mgah
2001 Jan 12 no. 16	15 993 - 26 632	NIST 2m	$CuSO_4$	Si	0.02	2.0	250	Ne	$3.41 \pm\ 0.04$	mgnh
2001 Mar 30	24 007 - 29 700	ICL UV	Glass	1P28	0.04	0.45	90	Ar	$2.26 \pm\ 0.017$	$_{ m mjah}$
2001 Mar 27	24 057 - 29 786	ICL UV	Glass	1P28	0.04	0.45	340	Ne	2.71 ± 0.05	mjnh
$2001~\mathrm{Mar}~27$	24779 - 27567	ICL UV	Glass	1P28	0.04	0.20	340	Ne	$2.47 \pm\ 0.06$	$_{ m mjnl}$
2001 Apr 02	25 421 - 41 943	ICL UV	UG5	1P28	0.04	0.45	90	Ar	1.80 ± 0.06	$_{ m mkah}$
2001 Mar 22	25 355 - 41 970	ICL UV	UG5	1P28	0.04	0.45	340	Ne	$2.41 \pm\ 0.05$	mknh
2001 Mar 26	35 690 - 35 770	ICL UV	UG5	1P28	0.04	0.20	340	Ne	2.76 ± 0.07	mknl
$2001 \; \mathrm{Apr} \; 02$	33 897 - 49 984	ICL UV	-	R166	0.04	0.45	90	Ar	$2.21 \pm\ 0.12$	mlah
2001 Mar 21 no. 2	33897 - 52425	ICL UV	-	R166	0.04	0.45	340	Ne	$2.21 \pm\ 0.16$	mlnh
2001 Mar 21 no. 1	35 770 - 35 806	ICL UV	-	R166	0.04	0.45	340	Ne	$2.26 \pm\ 0.21$	mlnl
2001 Dec 04	33 895 - 58 990	ICL VUV	BP185	R1220	0.05	0.45	340	Ne	$0.81 \pm\ 0.29$	mmnh
2012 Sep 13	33 897 - 58 990	ICL VUV	BP185	R1220	0.08	0.70	300	Ne	13.30 ± 0.50	-
1998 Nov 12 no. 6	21 480 - 37 910	NIST FT700	-	R106UH	0.06	2.00	133	Ne	-1.32 ± 0.10	-
1998 Nov 12 no. 2	36 800 - 47 510	NIST FT700	-	R7154	0.07	2.00	150	Ne	8.76 ± 0.10	-

NOTE—* $k_{\rm eff}$, calibration correction factor for the spectrum with its uncertainty, where superscript * indicates a newly revised $k_{\rm eff}$, detailed in Section 2.1.1. The uncertainty in $k_{\rm eff}$ is the propagated uncertainty through the calibration chain. †Name of spectrum as given in R. J. Blackwell-Whitehead (2003).

ratio. In these instances, we employed the HFS fitting routines in Xgremlin, originally developed by B. V. Pulliam (1979). These routines perform iterative fits using up to eight adjustable parameters: the magnetic dipole (A) and electric quadrupole (B) constants for both upper and lower levels, the central wavenumber, full width at half maximum (FWHM), Voigt profile damping factor, and signal-to-noise ratio. Parameters could be fixed to known values if available, and the software allowed simultaneous fitting of up to three overlapping transitions per spectral feature. The fitting process provided uncertainties for all derived parameters.

Wavenumber calibration was performed using 26 Ar II reference lines in the visible region (R. C. M. Learner & A. P. Thorne 1988), based on measurements by W. Whaling et al. (1995). Calibrated Mn lines from Mn–Ar spectra were then used to transfer the calibration to Mn–Ne spectra, extending coverage into the IR and VUV. Each step in this cross-calibration process introduces a cumulative uncertainty in the wavenumber positions. The total calibration uncertainty of a spectral line is the combination of the error in the applied calibration correction for each spectrum and the uncertainties of the initial reference wavenumbers, which trace back to the standards reported by W. Whaling et al. (1995) with an accuracy of approximately one part in 108. The

total wavenumber uncertainty of each spectral line is then the combination in quadrature of the calibration uncertainty of the line's spectrum with the statistical uncertainty of the line fit.

In total, 18,948 spectral lines were measured across all FT spectra. Multiple observations of the same line were merged using a weighted average, with weights inversely proportional to the signal-to-noise ratio. This yielded 10,432 unique lines in the final linelist, encompassing all species present in the HCL plasmas: Mn I, Mn II, carrier gases, cathode alloy constituents, and impurities.

2.1.1. Recalibration of IR FTS Spectra

It was noticed during the initial energy level optimisation that the values of the $3d^5(^6S)4s4p(^3P)$ z^6P levels were inconsistent, depending on whether they were determined via the ground level, $3d^54s^2$ $a^6S_{^5/2}$, with lines around 400 nm, or via the $(^5D)4s$ a^6D term with lines in the IR around 1350 nm. Accurate values for these levels not only set the foundation for the entire term system, but also determine improved wavelengths for parity-forbidden lines between the a^6S and a^6D terms.

Whilst there are various reasons why the lines from the z^6P term may be inconsistent, the large separation of the lines to the a^6S and a^6D terms led us to re-examine the wavenumber calibration of the IR spectra. Wavenumber calibration constants, $k_{\rm eff}$, are calcu-

lated from observed wavenumbers, $\sigma_{\rm obs}$, and reference wavenumbers, $\sigma_{\rm ref}$, where

$$k_{\text{eff}} = 1 - \sigma_{\text{obs}} / \sigma_{\text{ref}}$$
 (1)

These values are given in Table 3.2 of F. Liggins (2017) (hereafter L17), and in Table 1 of F. S. Liggins et al. (2021). Corresponding plots of the value of k_{eff} against wavenumber are given in Figs. 3.3 to 3.18 of L17. The primary wavenumber standards, given in Table 3.1 of L17, were 26 lines of Ar II from W. Whaling et al. (1995). Three spectra (mjah, mgah, and meah) were calibrated directly from these standards and the calibration plots are shown in Figs 3.3, 3.4, and 3.5 of L17 respectively. The remaining spectra were calibrated using strong, unblended, Mn lines found in these spectra, and the calibration chain is given in Table 3.5 of L17 and Table 1 of F. S. Liggins et al. (2021). This table shows that the three spectra in the IR (manh, maah, and mcnh) were all calibrated from the spectrum meah, whereas all the other spectra in Table 3.2 of L17 were calibrated via mjah, either directly or using overlapping spectra.

The calibration plots of mjah and meah are given in Figs 3.3 and 3.4 of L17 and are reproduced here in Fig. 1. It can be seen that while the value of $k_{\rm eff}$ is independent of wavenumber for spectrum mjah, the plot for spectrum meah shows a small slope of about $-6.2 \times 10^{-12} \sigma$ from 19 000 cm⁻¹ to 24 000 cm⁻¹. This slope would result in an error of 0.0007 cm⁻¹ at 7300 cm⁻¹, roughly three times the uncertainty of strong lines in this region. The wavelength-dependent nature of the deviation suggests that the issue with spectrum meah is more likely due to illumination shifts, rather than plasma effects, which would manifest as energy level dependent variations.

Fortunately, there are sufficient overlapping lines between spectrum mjnh, calibrated directly from mjah, and mcnh to provide a revised calibration for this spectrum that omits the problematic spectrum meah. This calibration is shown in Fig. 2, and has an offset of about 8 parts in 10^8 with respect to the value given in Table 3.2 of L17. The recalibrated spectrum mcnh was used to adjust the calibration of manh and maah in the IR region, and the calibration of meah and menh between $7000 \,\mathrm{cm}^{-1}$ to $18\,000 \,\mathrm{cm}^{-1}$. Details of the revised values of k_{eff} are given in Table 2. The values of k_{eff} for all other spectra are unchanged from Table 3.2 of L17 and Table 1 of F. S. Liggins et al. (2021), but the details of all spectra used in this work are included in Table 1 here for completeness.

It should be noted that very few lines of Mn II are affected by this change as lines of Mn II are typically

weaker than those of Mn I in the IR region and thus have statistical uncertainties larger than the calibration correction. Table 3 gives the lines of Mn II that have changed from F. S. Liggins et al. (2021) by more than one standard uncertainty following the recalibration of spectra described above.

2.2. Grating Spectroscopy

Grating spectra of a high-current, water-cooled hollow cathode lamp (HCL) were recorded over the range 28,385–121,728 cm⁻¹ (82 to 353 nm) using the 10.7 m normal-incidence vacuum spectrometer (NIVS) at NIST, USA. To suppress second-order diffraction from shorter wavelengths, MgF₂ or fused silica filters were used above 50,000 cm⁻¹. The HCL employed a Mn/Ni foil placed in a Cu cathode and was operated at a current of 2 A with 2 mbar of neon as the carrier gas. Spectra were recorded onto Kodak SWR photographic plates with 60-minute exposures. Full details are given in Table 2 of F. S. Liggins et al. (2021).

Spectral line positions were measured using a Grant Instruments spectrum plate comparator equipped with a digital encoder. In addition to positional measurements, a visual estimate of line intensity was recorded for each feature. These intensity estimates are approximate and should be regarded only as qualitative indicators of relative line strength.

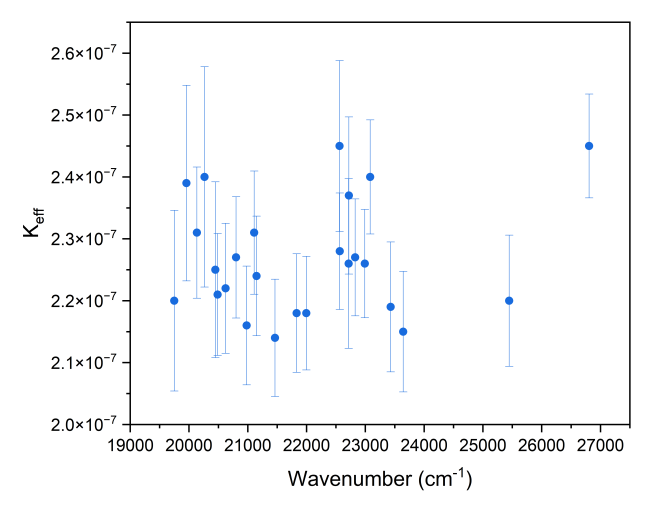
For wavelength calibration in the range 117–254 nm, spectra of a Pt–Ne HCL were recorded adjacent to the Mn exposures, allowing calibration via Pt standard lines (J. E. Sansonetti et al. 1992). For wavelengths below 117 nm, where no Pt–Ne spectra are available, calibration was performed using Cu II Ritz wavelengths derived from A. Kramida et al. (2017). For the remaining regions, Mn II Ritz wavelengths from F. S. Liggins et al. (2021) were used.

Uncertainties for each grating line were estimated based on line quality and photographic plate darkening. Lines with strengths between 5 and 60—sufficiently strong for accurate wavelength measurement but not saturated—were assigned an uncertainty of 0.0002 nm (equivalent to 0.05 cm⁻¹ at 50,000 cm⁻¹). Lines outside this range, or those exhibiting visual issues such as haze, broadening, or blending, were assigned a larger uncertainty of 0.0005 nm (0.125 cm⁻¹ at 50000 cm⁻¹).

In total, 10426 FTS + 11397 grating lines were included in the final linelist.

2.3. Grating Data from M. A. Catalán et al. (1964)

To supplement the new Mn I FTS and grating measurements, selected transitions from the historical line list of M. A. Catalán et al. (1964) were added to our



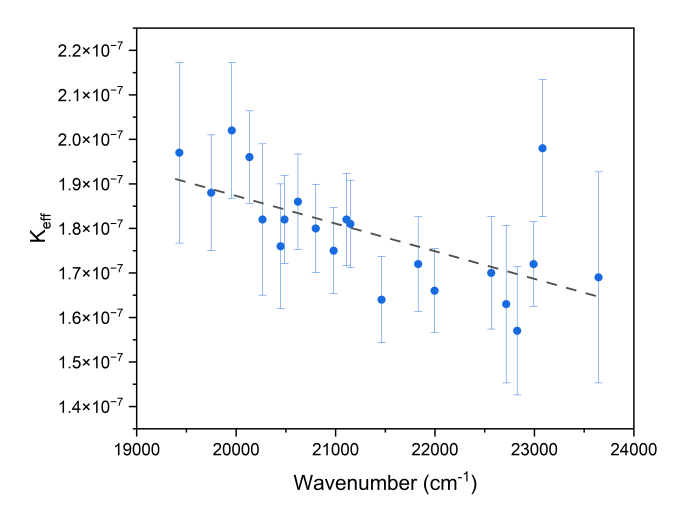


Figure 1. Original calibration of spectra mjah (left) and meah (right) using Ar II lines from F. Liggins (2017). The dotted line in the meah plot shows a linear fit to the k_{eff} data with a slope of -6.2×10^{-12} per cm⁻¹.

Table 2. Revised values of $k_{\rm eff}$ for IR FT spectra

Spectrum	Calibrated from	Old k as	Now h	S D	S.E.	S.E.prop	N	g/N .
Spectrum	Cambrated from	Old Keff	New Keff	Б.Д.	Б.Б.	J.E.prop	1 fit	5/1\min
		(10^{-7})	(10^{-7})	(10^{-8})	(10^{-8})	(10^{-8})		
mcnh	mjnh	1.68(5)	2.50(16)	7.62	1.62	2.1	22	50
manh	mcnh	1.31(11)	2.23(17)	7.01	1.65	3.8	18	50
maah	mcnh	2.50(9)	3.2(2)	9.71	2.23	4.1	19	50
menh	mcnh	1.49(4)	2.31(7)	9.25	0.69	2.8	180	50
meah	mcnh	1.78(3)	2.55(12)	7.95	1.18	3.3	45	50

Note—The old and newly revised $k_{\rm eff}$, calibration correction factors, for the listed IR spectra, with their standard deviation (S.D.) and standard error (S.E.). The final propagated standard error (S.E. $_{prop}$) is the propagated uncertainty through the calibration chain by linear addition of calibration uncertainty to that of the previous spectrum. N_{fit} is the number of lines used to calculate the calibration factor and S/N $_{min}$ gives the minimum S/N of the lines used in the calculation of $k_{\rm eff}$.

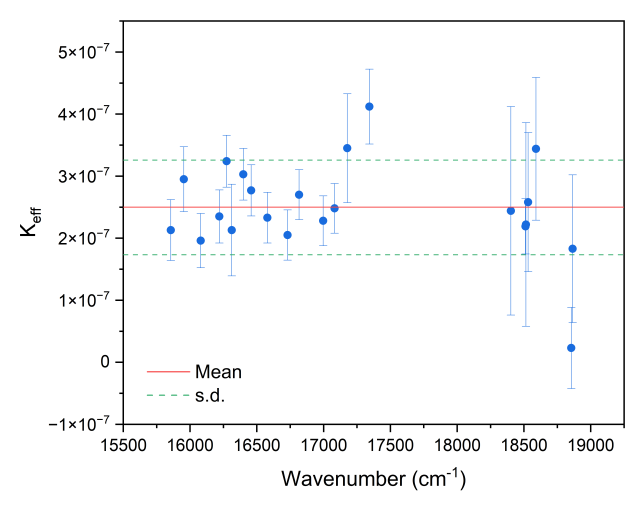


Figure 2. Recalibration of spectrum mcnh from mjnh for lines with $\mathrm{S/N} > 50$.

linelist. These transitions do not appear in any of the FTS or grating spectra described above, likely due to

differences in source conditions or measurement sensitivity. To ensure consistency, the wavelength calibration of the Mn I lines from M. A. Catalán et al. (1964) was carefully evaluated by matching common transitions to those observed in the FTS spectra. The distribution of wavelength differences was used to estimate wavelength uncertainties for Catalán's lines, as no uncertainties were reported in the original publication. Comparison plots between FTS wavelengths and Catalán's lines with no identified issues (given as line comments in M. A. Catalán et al. (1964)) and for lines with identified issues are given in Figure 3. There is a small offset of the mean wavelength difference of ~ 0.0018 Å in both plots, but as this shift is an order of magnitude less than the spectral line uncertainties, we decided not to shift the wavelengths given in M. A. Catalán et al. (1964).

Uncertainties for the Catalán lines were assigned based on qualitative assessments of line quality described in the original linelist. Lines flagged as problem-

Table 3. Classified Mn II line wavenumbers affected by the recalibration of IR FT spectra

Previous Wavenumber	Recalibrated Wavenumber	Trans	sition	Spectrum
(cm^{-1})	(cm^{-1})	Lower	Upper	-
6344.9269(5)	6344.9274(5)	$3d^5(^6S)4d \ e^7D_{3/2}$	$3d^5(^6S)5p \ x^7P_{2/2}^{\circ}$	mcnh
6401.9860(4)	6401.9865(4)	$3d^5(^6S)4d \ e^7D_{4/2}$	$3d^5(^6S)5p \ x^7P_{3/2}^{\circ}$	mcnh
6488.2264(4)	6488.2269(4)	$3d^5(^6S)4d \ e^7D_{5/2}$	$3d^{5}(^{6}S)5p \ x^{7}P_{4/2}^{\circ}$	mcnh
7745.6913(4)	7745.6919(4)	$3d^5(^6S)5d^{-5}D_{2/2}$	$3d^5(^6S)5f^{-5}F_{3/2}^{\circ}$	mcnh
7752.6648(4)	7752.6654(4)	$3d^5(^6S)5d^{-5}D_{3/2}$	$3d^{5}(^{6}S)5f^{-5}F_{4/2}^{\circ}$	mcnh
7760.5387(4)	7760.5393(4)	$3d^5(^6S)5d^{-5}D_{4/2}$	$3d^{5}(^{6}S)5f^{-5}F_{5/2}^{\circ}$	mcnh
8505.6310(4)	8505.6317(4)	$3d^{5}(^{6}S)5d^{-7}D_{5/2}$	$3d^{5}(^{6}S)5f^{-7}F_{6/2}^{\circ}$	menh
8510.8928(4)	8510.8935(4)	$3d^{5}(^{6}S)5d^{-7}D_{4/2}$	$3d^{5}(^{6}S)5f^{-7}F_{5/2}^{\circ}$	menh
` '	10090.7480(6)	$3d^{5}(^{6}S)4f^{-5}F_{5/2}^{\circ}$	$3d^{5}(^{6}S)5g^{-5}G_{6/2}$	
10090.7472(6)	· /			mcnh
10131.9471(6)	10131.9479(6)	$3d^5(^6S)4f^{-7}F_{1/2}^{\circ}$	$3d^5(^6S)5g^{-7}G_{1/2}$	mcnh
10132.0498(6)	10132.0506(6)	$3d^5(^6S)4f^{-7}F_{2/2}^{\circ}$	$3d^5(^6S)5g^{-7}G_{1/2}$	mcnh
10132.1628(6)	10132.1636(6)	$3d^5(^6S)4f^{-7}F_{1/2}^{\circ}$	$3d^5(^6S)5g^{-7}G_{2/2}$	mcnh
10132.2471(7)	10132.2479(7)	$3d^5(^6S)4f^{-7}F^{\circ}_{2/2}$	$3d^5(^6S)5g^{-7}G_{3/2}$	mcnh
10132.3160(5)	10132.3168(5)	$3d^{5}(^{6}S)4f^{7}F_{3/2}^{\circ}$	$3d^5(^6S)5g^{-7}G_{4/2}$	mcnh
10132.3777(5)	10132.3785(5)	$3d^5(^6S)4f^{-7}F^{\circ}_{5/2}$	$3d^5(^6S)5g^{-7}G_{6/2}$	mcnh
10132.4341(5)	10132.4349(5)	$3d^5(^6S)4f^{-7}F_{4/2}^{\circ}$	$3d^5(^6S)5g^{-7}G_{5/2}$	mcnh
10132.4341(5)	10132.4349(5)	$3d^5(^6S)4f^{-7}F^{\circ}_{6/2}$	$3d^5(^6S)5g^{-7}G_{7/2}$	mcnh
10523.0477(5)	10523.0486(5)	$3d^5(^6S)5s \ e^5S_{2/2}$	$3d^5(^6S)5p \ w^5P_{3/2}^{\circ}$	menh
10562.1796(5)	10562.1805(5)	$3d^5(^6S)5s\ e^5S_{2/2}$	$3d^5(^6S)5p\ w^5P_{2/2}^{\circ}$	menh
10586.3327(5)	10586.3336(5)	$3d^5(^6S)5s \ e^5S_{2/2}$	$3d^5(^6S)5p \ w^5P_{1/2}^{\circ}$	menh
11335.3143(6)	11335.3152(6)	$3d^5(^6S)5s \ e^7S_{3/2}$	$3d^5(^6S)5p \ x^7P_{2/2}^{\circ}$	mcnh
11400.4485(6)	11400.4494(6)	$3d^5(^6S)5s \ e^7S_{3/2}$	$3d^5(^6S)5p \ x^7P_{3/2}^{\circ}$	mcnh
11497.4267(6)	11497.4276(6)	$3d^5(^6S)5s \ e^7S_{3/2}$	$3d^5(^6S)5p \ x^7P_{4/2}^{\circ}$	mcnh
13751.8292(7)	13751.8303(7)	$3d^5(^6S)5p \ w^5P_{2/2}^{\circ}$	$3d^5(^6S)5d^{-5}D_{3/2}$	mcnh
13784.7483(7)	13784.7494(7)	$3d^5(^6S)5p \ w^5P_{3/2}^{\circ}$	$3d^5(^6S)5d^{-5}D_{4/2}$	mcnh
13790.9586(11)	13790.9597(11)	$3d^5(^6S)5p \ w^5P_{3/2}^{\circ}$	$3d^{5}(^{6}S)5d^{-5}D_{3/2}$	mcnh
13841.5649(8)	13841.5660(8)	$3d^5(^6S)5p \ x^7P_{4/2}^{\circ}$	$3d^5(^6S)5d^{-7}D_{4/2}$	mcnh
13846.7023(7)	13846.7034(7)	$3d^{5}(^{6}S)5p \ x^{7}P_{4/2}^{\circ}$	$3d^{5}(^{6}S)5d^{-7}D_{5/2}$	mcnh
13931.8750(11)	13931.8761(11)	$3d^{5}(^{6}S)5p \ x^{7}P_{3/2}^{\circ}$	$3d^{5}(^{6}S)5d^{-7}D_{2/2}$	mcnh
13938.5424(7)	13938.5435(7)	$3d^{5}(^{6}S)5p \ x^{7}P_{3/2}^{\circ}$	$3d^{5}(^{6}S)5d^{-7}D_{4/2}$	mcnh
13995.2053(7)	13995.2064(7)	$3d^{5}(^{6}S)5p \ x^{7}P_{2/2}^{\circ}$	$3d^{5}(^{6}S)5d^{-7}D_{1/2}$	menh
13997.0068(7)	13997.0079(7)	_ ′	$3d^{5}(^{6}S)5d^{-7}D_{2/2}$	
` '	13999.7959(7)	$3d^{5}(^{6}S)5p \ x^{7}P_{2/2}^{\circ}$ $3d^{5}(^{6}S)5p \ x^{7}P_{2/2}^{\circ}$, ,	mcnh
13999.7948(7)	· /		$3d^5(^6S)5d^{-7}D_{3/2}$	mcnh
16306.5871(8)	16306.5884(8)	$3d^5(^6S)4d \ e^5D_{1/2}$	$3d^5(^6S)4f^{-5}F^{\circ}_{2/2}$	menh
16311.2760(13)	16311.2773(13)	$3d^5(^6S)4d \ e^5D_{2/2}$	$3d^5(^6S)4f$ $^5F^{\circ}_{2/2}$	menh
16312.0712(8)	16312.0725(8)	$3d^5(^6S)4d \ e^5D_{2/2}$	$3d^5(^6S)4f$ $^5F_{3/2}^{\circ}$	menh
16318.7747(10)	16318.7760(10)	$3d^5(^6S)4d \ e^5D_{3/2}$	$3d^5(^6S)4f^{-5}F_{3/2}^{\circ}$	menh
16319.7153(8)	16319.7166(8)	$3d^5(^6S)4d \ e^5D_{3/2}$	$3d^5(^6S)4f^{-5}F_{4/2}^{\circ}$	menh
16327.8551(13)	16327.8564(13)	$3d^5(^6S)4d \ e^5D_{4/2}$	$3d^5(^6S)4f^{-5}F_{4/2}^{\circ}$	menh
16328.8579(8)	16328.8592(8)	$3d^5(^6S)4d \ e^5D_{4/2}$	$3d^5(^6S)4f^{-5}F^{\circ}_{5/2}$	menh
16890.3253(9)	16890.3267(9)	$3d^5(^6S)4p \ z^7P_{4/2}^{\circ}$	$3d^44s^2 \ c^5D_{4/2}$	mcnh, men mgnh, k1
17289.8857(10)	17289.8871(10)	$3d^5(^4F)4p \ x^5D^{\circ}_{4/2}$	$3d^5(^6S)5d^{-7}D_{3/2}$	mcnh, menl mgnh, mga meah, k1

atic (e.g. hazy, broadened, or blended) were assigned an uncertainty of 0.003 nm, while all other lines were given an estimated uncertainty of 0.001 nm. In total, 718 Mn I lines from M. A. Catalán et al. (1964) were not found in our grating or FTS spectra and were therefore included in our initial energy level analysis. Of these, 415 lines were used directly to support level identifications, and resolve ambiguities in term assignments. No energy levels in this work were determined using transitions observed exclusively in the Catalán spectra.

2.4. Final Linelist

The final linelist compiled for this work includes transitions from FT spectroscopy, grating spectroscopy, and selected grating historical measurements. In total, 24237 unique spectral lines were identified and characterised, spanning a broad wavenumber range, from 1820 cm⁻¹ to 121717 cm⁻¹ (821 nm to 54916 nm). Each line was assigned a wavenumber, relative intensity, S/N, FWHM, and a wavenumber uncertainty based on the measurement method and line quality. This comprehensive linelist forms the basis for the term analysis of Mn I presented in this work.

3. Mn I SPECTRAL ANALYSIS

3.1. Line Identification

The first stage of the term analysis of Mn I involved identifying transitions in the compiled linelist. Transitions were observed from neutral and singly ionised manganese (Mn I and Mn II), as well as from carrier gases and impurity elements originating from the cathode alloys used in the HCLs.

Initial identification of Mn I lines was carried out by comparing observed wavenumbers with Ritz values derived from the compiled energy levels of S&C. Mn II transitions were identified using Ritz wavenumbers based on the extensive energy levels of F. S. Liggins et al. (2021). Together, Mn I and Mn II lines accounted for the vast majority of observed transitions.

Carrier gas lines were identified using published references: Ar I and Ar II from W. Whaling et al. (2002, 1995), Ne I from E. B. Saloman & C. J. Sansonetti (2004), and Ne II from A. Kramida & G. Nave (2006). Impurity lines from cathode alloy constituents were identified using U. Litzén et al. (1993) for Ni I, C. P. Clear et al. (2022, 2023) for Ni II, A. Kramida et al. (2019) for Cu I, and A. Kramida et al. (2017) for Cu II.

In the grating spectra above 120 nm, spectral lines of Ni II and Cu II were generally weak due to poor excitation of these species in neon under those conditions. However, strong Cu II lines were observed below 120 nm, attributed to the high population of low-lying levels of Cu II facilitated by the Ne carrier gas.

The complex term analysis process, described in sections 4, 5 and 6, is iterative, and results eventually in a final spectrum linelist of identified Mn I lines.

3.2. The Mn I Spectrum

After the term analysis procedure, in total, 2186 spectral lines have been classified as Mn I transitions. Of these, 1642 lines were measured using high-resolution FTS. A small number of lines have been multiply identified where a single assignment could not be conclusively made.

All observed classified Mn I transitions are listed in Table 4. The first column indicates the method of spectral line measurement, with a key provided in the table footnote. The second column gives the integrated relative intensity of each line. For FTS lines, designated "F", intensities were calibrated using standard lamp spectra. Grating lines recorded on photographic plates, designated "G", have intensities based on visual estimates of plate darkening. Notes on line appearance (e.g. hazy, broadened, blended) are indicated by appended letters, with definitions provided in the footnote. For lines from M. A. Catalán et al. (1964), designated "C", intensities are taken directly from their paper. Direct comparisons between intensities from different measurement methods should not be made.

Columns 3 and 4 list the FWHM (in cm⁻¹) and S/N for FTS lines. Columns 5 through 7 give the observed wavelength in air and vacuum, and the associated wavelength uncertainty. Air wavelengths are listed for transitions between 200 nm and 2 μ m and are derived from vacuum wavelengths using the five-parameter dispersion formula of E. R. Peck & K. Reeder (1972). Observed wavenumbers and their uncertainties are presented in columns 8 and 9. Columns 10 and 11 contain Ritz wavenumbers and uncertainties, calculated from the optimised energy levels determined in this work. Values in columns 5, 6, 8, and 10 have been rounded according to the "rule of 25," ensuring that the uncertainty in the final digit does not exceed 25.

The upper and lower energy level designations for each transition are given in columns 12 and 13, with their corresponding optimised energy values listed in columns 14 and 15. The final column provides notes on individual lines, including indications of blending, poor line quality, or lines assigned reduced weights during the energy level optimisation.

4. ATOMIC STRUCTURE OF Mn I

Mn I belongs to the iron-group (3d) elements and has a ground level configuration of $3d^54s^2 a^6S_{5/2}$. In

Table 4. Classified Lines of Mn I

Source	Int.	FWHM	S/N	λ_{air}	λ_{vac}	Unc.	$\sigma_{obs.}$	Unc.	σ_{Ritz}
		(10^{-3}cm^{-1})		(nm)	(nm)	(nm)	(cm^{-1})	(cm^{-1})	(cm^{-1})
F	2.41	39	6	-	51112.337	0.015	1956.478	0.007	1956.475
F	2.62	45	8	-	51046.145	0.019	1959.000	0.005	1959.012
F	2.25	14	10	-	51006.649	0.018	1960.5277	0.0024	1960.529
F	3.09	56	20	-	48638.746	0.011	2055.9749	0.0024	2055.974
F	2.92	50	15	-	48554.536	0.012	2059.531	0.003	2059.540
F	2.89	52	14	-	45082.664	0.010	2218.145	0.003	2218.148
F	3.03	43	23	-	42880.46	0.03	2332.0644	0.0019	2332.064
F	3.18	73	19	-	42744.85	0.05	2339.464	0.003	2339.463
F	3.10	52	37	-	42570.38	0.03	2349.055	0.003	2349.0511
F	2.89	37	29	-	42432.76	0.03	2356.677	0.005	2356.6696
F	2.96	22	11	-	41895.916	0.024	2386.869	0.003	2386.8675
F	2.85	59	11	-	41551.11	0.04	2406.682	0.004	2406.6745
F	1.82	19	3	-	37961.394	0.016	2634.254	0.009	2634.2552
F	2.58	63	5	-	37936.913	0.016	2635.951	0.006	2635.9551
F	2.72	57	8	-	37923.49	0.05	2636.884	0.008	2636.888
F	2.51	50	6	-	37367.797	0.008	2676.111	0.005	2676.1011
F	2.63	46	8	-	37302.184	0.008	2680.8065	0.0014	2680.8082
F	3.00	23	67	-	36789.558	0.014	2718.1636	0.0020	2718.1626
F	2.99	42	22	-	36753.018	0.016	2720.872	0.005	2720.8650
F	2.84	59	11	-	36730.071	0.017	2722.562	0.016	2722.5649

Unc.	Lower Level		Upper Level			E_L	E_U	Notes	
(cm^{-1})	Config.	Term	J	Config.	Term	J	(cm^{-1})	(cm^{-1})	
0.0005	$3d^{6}(^{5}D)4p$	x^6P	$^{3/2}$	$3d^{5}4s(^{7}S)4d$	x^6P	5/2	45259.1735	47215.6484	
0.0007	$3d^6(^5D)4p$	x^6P	$^{3/2}$	$3d^{5}4s(^{7}S)4d$	x^6P	$^{3/2}$	45259.1735	47218.1853	
0.0007	$3d^6(^5D)4p$	x^6P	$^{3/2}$	$3d^54s(^7S)4d$	x^6P	$^{1}/_{2}$	45259.1735	47219.7023	
0.0005	$3d^6(^5D)4p$	x^6P	5/2	$3d^54s(^7S)4d$	x^6P	7/2	45156.1085	47212.0826	
0.0005	$3d^6(^5D)4p$	x^6P	5/2	$3d^54s(^7S)4d$	x^6P	5/2	45156.1085	47215.6484	
0.0005	$3d^6(^5D)4p$	x^6P	7/2	$3d^54s(^7S)4d$	x^6P	7/2	44993.935	47212.0826	
0.0019	$3d^54s(^7S)6s$	f^8S	7/2	$3d^54s(^7S)6p$	f^8S	5/2	50157.7535	52489.8179	
0.003	$3d^54s(^7S)6s$	f^8S	7/2	$3d^54s(^7S)6p$	f^8S	7/2	50157.7535	52497.217	
0.0017	$3d^54s(^7S)6s$	f^8S	7/2	$3d^54s(^7S)6p$	f^8S	9/2	50157.7535	52506.8046	
0.0014	$3d^54s(^7S)6s$	g^6S	5/2	$3d^54s(^7S)6p$	g^6S	7/2	50904.607	53261.2766	
0.0014	$3d^54s(^7S)6s$	g^6S	5/2	$3d^54s(^7S)6p$	g^6S	5/2	50904.607	53291.4745	
0.0024	$3d^54s(^7S)6s$	g^6S	5/2	$3d^54s(^7S)6p$	g^6S	$^{3/2}$	50904.607	53311.282	
0.0011	$3d^5(^4P)4s4p(^3P)$	v^6P	$^{3/2}$	$3d^54s(^7S)5d$	v^6P	5/2	50099.2245	52733.4797	
0.0011	$3d^5(^4P)4s4p(^3P)$	v^6P	3/2	$3d^54s(^7S)5d$	v^6P	3/2	50099.2245	52735.1796	
0.003	$3d^5(^4P)4s4p(^3P)$	v^6P	$^{3/2}$	$3d^54s(^7S)5d$	v^6P	$^{1/2}$	50099.2245	52736.112	
0.0006	$3d^54s(^7S)4d$	e^6D	7/2	$3d^5(^4P)4s4p(^3P)$	e^6D	7/2	47212.0826	49888.1836	
0.0006	$3d^54s(^7S)4d$	e^6D	9/2	$3d^5(^4P)4s4p(^3P)$	e^6D	7/2	47207.3755	49888.1836	
0.0010	$3d^5(^4P)4s4p(^3P)$	v^6P	5/2	$3d^54s(^7S)5d$	v^6P	7/2	50012.6147	52730.7773	
0.0012	$3d^{5}(^{4}P)4s4p(^{3}P)$	v^6P	5/2	$3d^{5}4s(^{7}S)5d$	v^6P	5/2	50012.6147	52733.4797	
0.0013	$3d^5(^4P)4s4p(^3P)$	v^6P	$\frac{5}{2}$	$3d^{5}4s(^{7}S)5d$	v^6P	$^{3}/_{2}$	50012.6147	52735.1796	

Note—Note. The columns are: (1) the source of the line: F - FT spectra, G - grating spectra, C - from M. A. Catalán et al. (1964). (2) relative line intensity. Ft intensity is the log of the relative line intensity. Intensities from the FT and grating spectra are on different scales. Photographic plate line intensities are visual estimates of plate darkening, with qualifiers: w—wide, b—broad, s—shaded to short wavelengths, l—shaded to long wavelengths, p—perturbed (e.g., on a wing of a stronger line), h—hazy, q—questionable position, c—complex (central position is blend of 3 or more lines). (3) full width at half maximum (for FT lines only). (4) signal-to-noise ratio (for FT lines only). (5) Ritz air wavelength given for lines between 200 nm and 2 \(\mu\max{m}\max{m}\) (6) Ritz vacuum wavelength. (7) Ritz wavelength uncertainty. (8) observed wavenumber. (9) observed wavenumber uncertainty. (10) Ritz wavenumber, derived from the optimised upper and lower energy level values of the transition. (11) Ritz wavenumber uncertainty. (12-14) configuration, term and J of the lower energy level. (15-17) configuration, term and J of the upper energy level. (18) lower energy level value. (19) upper energy level. (20) notes associated with the line: multiply classified with Mn I, Mn II or Mn III ("I", "III"), or another element (e.g. Ar, Ne, Cu). Lines with '\(\pm\) were assigned a lower weight in the energy level optimisation. Hindicates lines that were fitted with HFS parameters to determine observed wavenumbers. (This table is available in its entirety in machine-readable form)

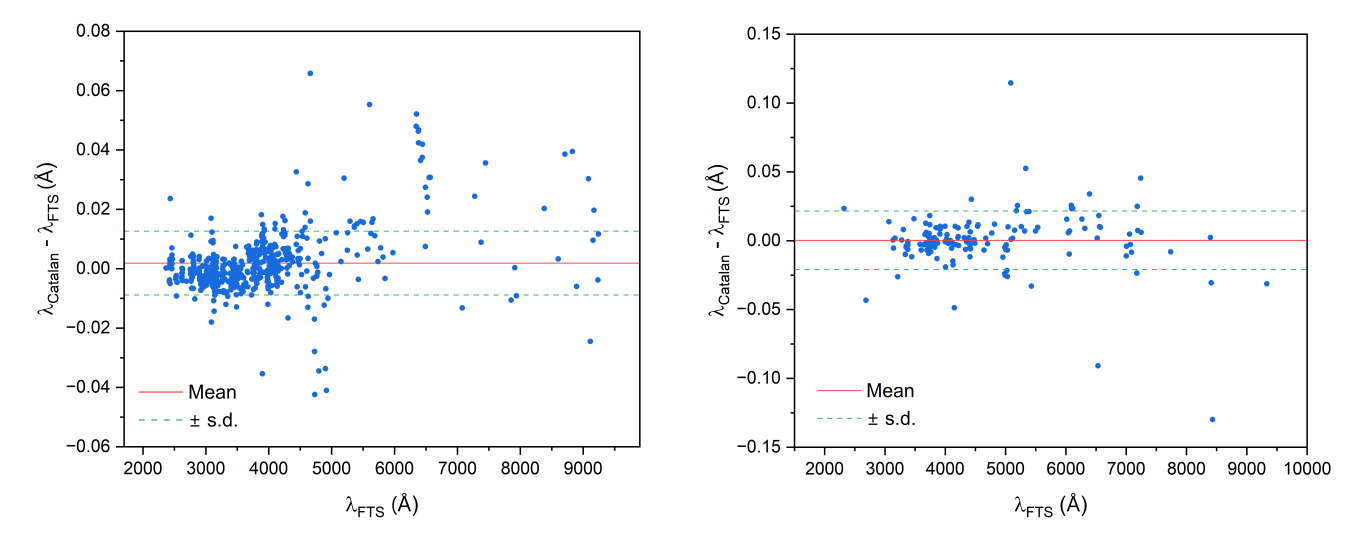


Figure 3. Comparisons between previously published grating wavelengths (M. A. Catalán et al. 1964) and FTS wavelengths (F. S. Liggins et al. 2021). Left: Lines with no identified issues. Right: Lines with issues (e.g. hazy, broadened).

these elements, the nd and (n+1)s electron configurations have similar binding energies, resulting in significant overlap between the three lowest configurations of Mn I: $3d^7$, $3d^64s$, and $3d^54s^2$. This overlap leads to observable two-electron transitions due to configuration interaction among these low-lying states. Within each configuration, strong mixing between LS components allows transitions between normally forbidden intercombination lines, enabling the entire term system of Mn I to be connected to its ground state.

The energy level structure of Mn I is divided into two major configuration systems. The singly excited (or "normal") system consists of one valence electron in the $3d^6(^ML)nl$ subconfigurations, built on the parent terms $3d^6(^ML)$ of Mn II. A schematic diagram of this system is shown in Figure 4, where subconfigurations are grouped by their parent terms from the Mn II ground state. Each box in Figure 4 represents the energy range of levels within a given subconfiguration. The 3F and 3P parent terms appear twice in the diagram, differentiated by index numbers. The parent terms 1H , 1F , and 3S are not included as they are neither known in Mn II nor associated with any observed classified transitions in Mn I.

The doubly excited system of Mn I contains two valence electrons in the $3d^5(^ML)nl\,n'l'$ subconfigurations and is built on the grandparent terms $3d^5(^ML)$ of Mn III. A schematic diagram of this system is shown in Figure 5. As in the singly excited system, most levels below the ${}^{7}S_{3}$ ionisation limit are known, and a large fraction belong to the $3d^5(^6S)$ grandparent ground state system. In S&C, this 6S grandparent term is described using three different term labels: ⁷S, ⁵S, and ⁶S. The $3d^5(^6S)4s4p$ configuration is assigned to the 6S grandparent term, while configurations above $3d^54s4p$ are described as $3d^54s(^7S)n'l'$ or $3d^54s(^5S)n'l'$. An expanded schematic diagram of the $({}^{6}S)$ parent term is shown in Figure 6. This (^{7}S) or (^{5}S) description originates from the level identifications of M. A. Catalán et al. (1964). For clarity and consistency we have retained this nomenclature, and our optimised energy levels are classified using these original term designations.

In the neutral spectrum of manganese, the doubly excited system dominates, with 314 observed levels assigned to doubly excited configurations. In total, excluding the new levels found in this work, there are 550 previously known levels of Mn I (J. Sugar & C. Corliss 1985). The doubly excited system constitutes approximately 65% of the known levels with the singly excited system accounting for approximately 33% . The remaining $\sim\!\!2\%$ of known levels are not classified and have no assigned configuration in previously published

work. The majority of these levels are above the $^{7}S_{3}$ limit and have considerable mixing with other levels.

It should be noted that 97 of the previously observed levels in the doubly excited system form part of the Rydberg series for the 7S_3 and 5S_2 limits. These high order np configurations do not have transitions in a majority of astrophysical spectra and are mainly used in the calculation of the ionisation limit of the ground configurations. These levels were not populated in our laboratory spectra and are not included in this analysis.

5. ENERGY LEVEL OPTIMISATION

Observed wavenumbers and their associated uncertainties were used in a least-squares fitting procedure with the program LOPT (A. E. Kramida 2011) to confirm and optimise previously known energy levels of Mn I. Each Mn I transition was weighted by the inverse square of its total wavenumber uncertainty. Transitions with multiple identifications were initially assigned low weightings (i.e. high uncertainties), ensuring that line parameters were retained in the dataset but did not influence the optimisation of energy level values. These weightings were revised as identifications were resolved.

The optimisation process was iterative. It commenced with a small subset of low-lying odd energy levels that exhibited strong transitions to the ground state. Once optimised, these levels were then used to refine the identification of additional Mn I transitions in the linelist. The process was then repeated for further subsets of energy levels, progressively expanding the number of identified transitions. At each stage, any observed wavenumber that deviated significantly from its Ritz wavenumber (calculated from fitted energy levels) was investigated for possible misidentification, blending, or HFS. In such cases, the line identification was removed, the weighting reduced, or the spectral line remeasured, respectively. This iterative procedure was continued until all previously known energy levels that could be confirmed were optimised. A detailed search was then performed for new energy levels associated with previously unclassified spectral lines. Details of discovery of new levels are given in Section 6.

All energy level values, both revised and newly identified, are presented in Table 5. Columns one through three list the configuration, term, and J-value of each energy level. Columns four and five give the optimised energy and its uncertainty, relative to the ground state. Flags indicating special cases (e.g. uncertain identifications, blended levels) are given in column six, with definitions provided in the table footnote. The final column lists the total number of transitions used in the optimisation of each level.

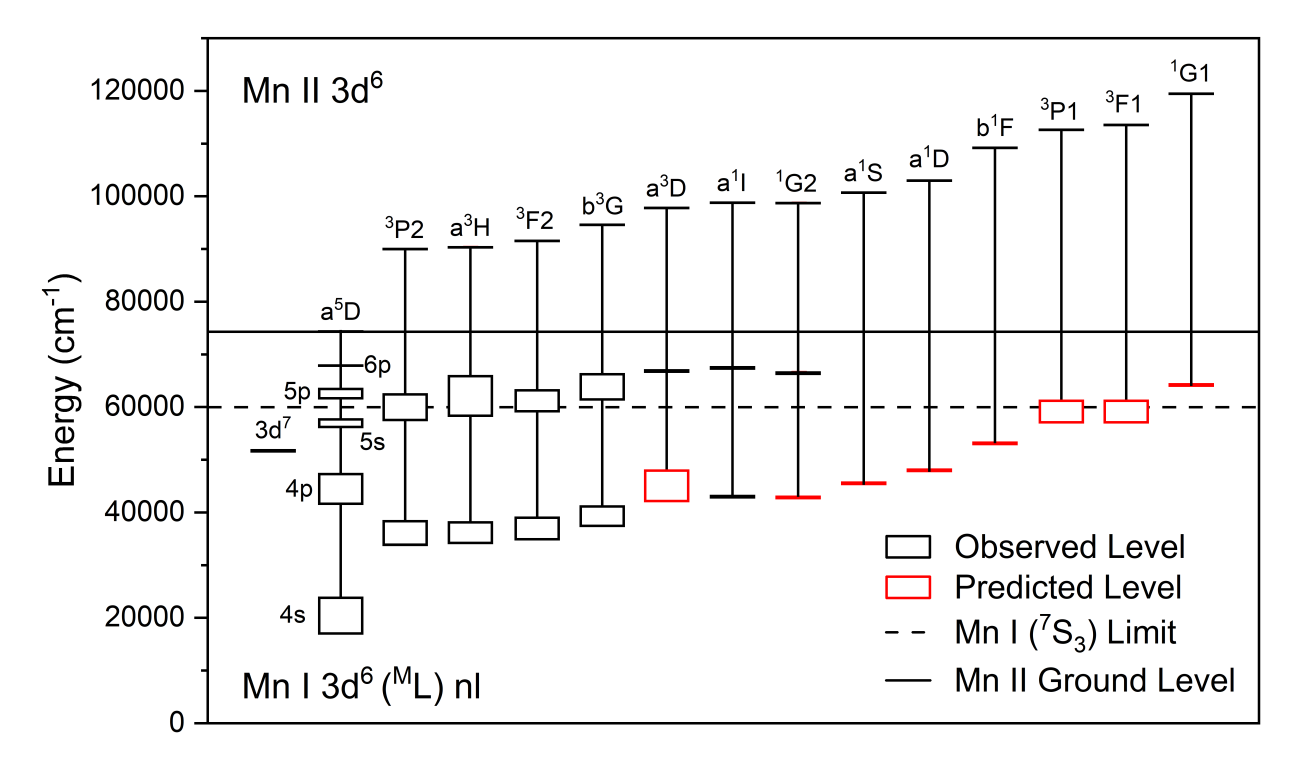


Figure 4. The singly excited system of energy levels in Mn I.

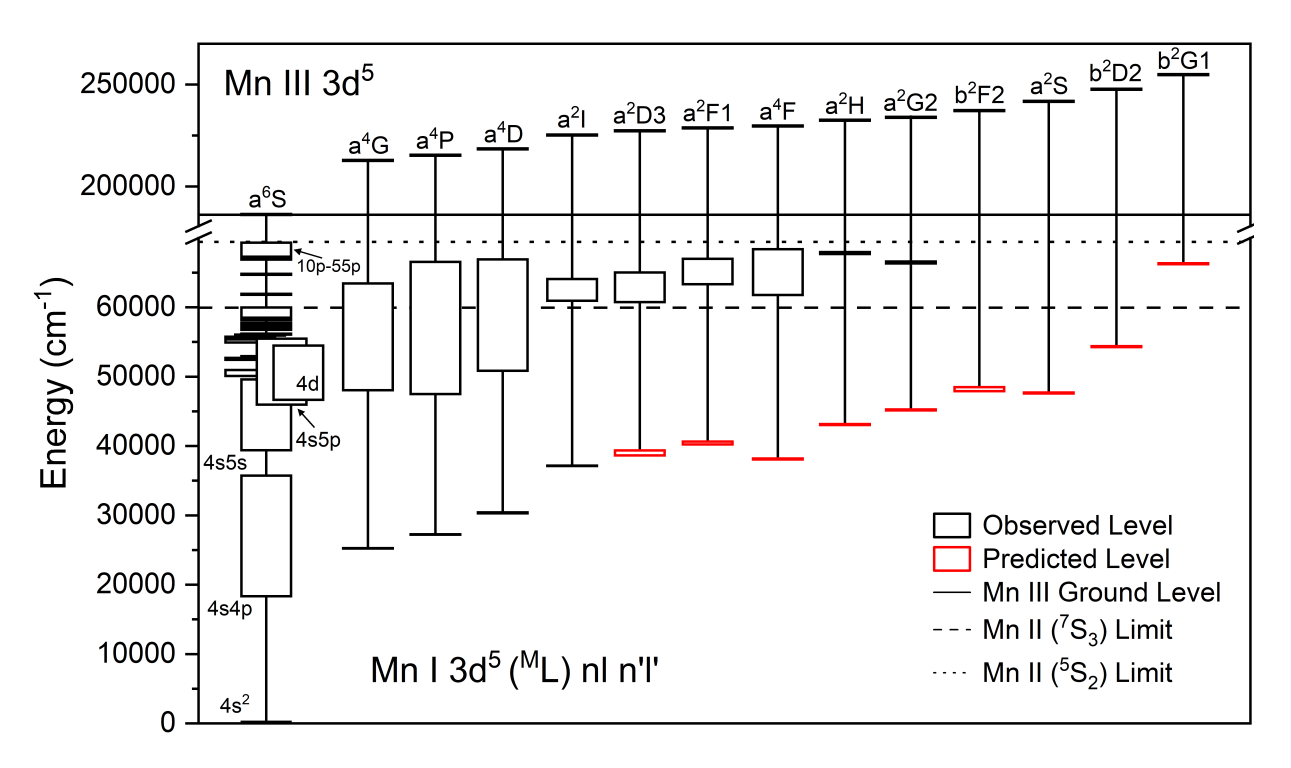


Figure 5. The doubly excited system of energy levels in Mn I.

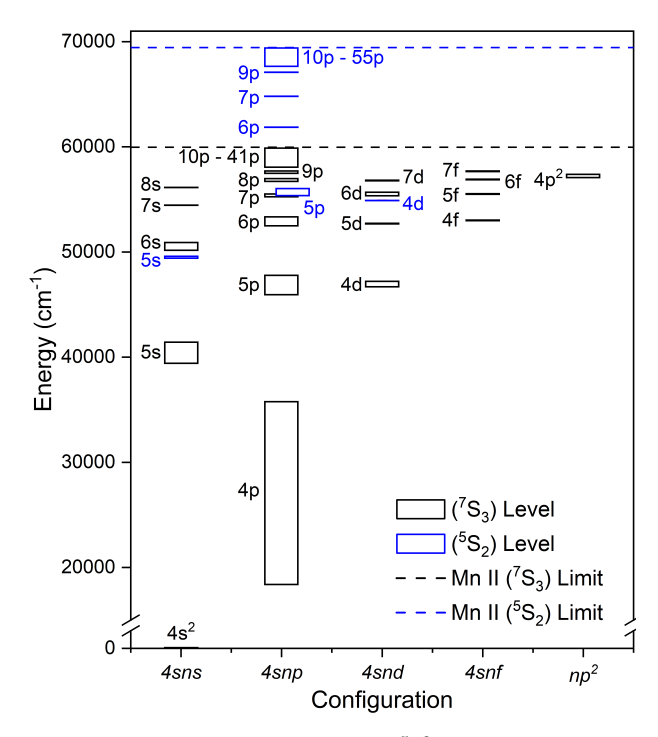


Figure 6. Expanded view of the $3d^5(^6S)nl\,n'l'$ subconfiguration.

The uncertainty of the energy levels is the uncertainty of the level structure least squares fit from LOPT with the linear addition of the uncertainty of the original Ar II standard lines (1 part in 10^8). This is because the uncertainty of the standard lines is common to all observed lines and thus it becomes weighted out of the least squares fit and the resultant level uncertainties during level optimisation. We have adopted a global calibration uncertainty, based on the maximum calibration uncertainty in Table 1, of 3 parts in 10⁸ (from spectrum mmnh). We did not adopt the 5 parts in 10⁸ global calibration uncertainty used in F. S. Liggins et al. (2021) which was based on the calibration uncertainty of spectrum "2012 Sep 13", as the hollow cathode discharge source for this spectrum was optimised for Mn II and only produced a small number of weak Mn I lines that were used in our analysis. Our global calibration uncertainty was set as the minimum uncertainty for all optimised energy level values and Ritz wavenumbers.

A discussion of the energy levels listed in S&C which have been confirmed and optimised, with substantial reductions in uncertainties, following our analysis is given in the following sections. The designations of 52 energy levels have also been redesignated following our analysis and are detailed in Table 6.

5.1. The Even Levels of the Singly Excited System 5.1.1. The 3d⁷ and 3d⁶(^ML)4s configurations

As in S&C, only the three levels of the $3d^{7}$ ^{4}P term have been found for this configuration. There were no lines present in our spectra for transitions to the remaining terms of the $3d^{7}$ configuration.

All of the levels of the $3d^6(^ML)4s$ subconfiguration for the $(^5D), (^3P_2), (^3H), (^3F_2), (^3G)$ and (^1I) parent terms in S&C have been identified and optimised following our analysis, and these subconfigurations are now complete. No transitions to the levels of the remaining parent term 4s subconfigurations were present in our spectra, and these levels remain unknown.

5.1.2. The $3d^6(^5D)5s$ and $3d^6(^5D)4d$ subconfigurations

No energy levels corresponding to the configurations $3d^65s$ or $3d^64d$ arising from parent terms higher than $3d^6(^5D)$ are reported in Sugar and Corliss (S&C). Consistent with this, all levels identified in our analysis for these configurations also originate exclusively from the $3d^6(^5D)$ parent term. For the $(^5D)5s$ levels, we have assigned the levels of the e^4D term, which were given without configurations in S&C as $(^5D)5s$ e^4D . The $(^5D)5s$ $e^4D_{3/2}$, in S&C at 56601.63 cm⁻¹, was discarded and replaced by a new level value at 56617.4657 cm⁻¹. The $(^5D)5s$ e^4D term remains incomplete with $e^4D_{1/2}$ still unknown. The same is true for the $(^5D)5s$ i^6D term with with $i^6D_{1/2}$ missing. We have redesignated the levels labelled as $(^5D)5s$ f^4D in S&C as $3d^6(^5D)5s$ f^4D levels.

For the $(^5D)4d$ subconfigurations, the following levels in S&C could not be confirmed with the lines present in our FT or grating spectra: $e^4F_{9/2, 7/2}$, $e^6F_{3/2}$ and $e^6G_{5/2, 3/2}$. The remaining S&C levels of the $(^5D)4d$ subconfiguration have all been confirmed and optimised following our analysis.

5.2. The Odd Levels of the Singly Excited System 5.2.1. The 3d⁶(^ML)4p subconfigurations

In total, 90% of the levels of the $3d^6(^ML)4p$ subconfigurations listed in S&C have been confirmed and optimised following our analysis. The $3d^6(^5D)4p$ subconfiguration is complete, as is the $3d^6(^3H)4p$ subconfiguration with levels now assigned to the designations $3d^6(^3H)4p$ $v^4G_{5/2}$ and $v^4G_{7/2}$ at 65873.2859 cm⁻¹ and 65876.2678 cm⁻¹ respectively. The S&C level $3d^6(^3F)4p$ $^2F_{5/2}$ at 61469.70 cm⁻¹ has been discarded and replaced with a new level found at 61471.2400 cm⁻¹. 10 levels were not optimised in our analysis due to the lack of new FT or grating lines in our spectra. These mostly belong to the $3d^6(^3G)4p$ subconfiguration, with 2 levels from the $3d^6(^3D)4p$ subconfiguration and 1 from

Table 5. Energy Levels of Mn I

Ener	gy Leve	l		E	Unc.	Flag	No. of
Configuration	Term	J	Parity	(cm^{-1})	$({\rm cm}^{-1})$		Lines
$3d^{5}4s^{2}$	a^6S	5/2	even	0.0	0.0		77
$3d^6(^5D)4s$	a^6D	9/2	even	17052.3043	0.0005		46
$3d^6(^5D)4s$	a^6D	$^{7/2}$	even	17282.0213	0.0005		77
$3d^6(^5D)4s$	a^6D	5/2	even	17451.5369	0.0005		80
$3d^6(^5D)4s$	a^6D	$^{3}/_{2}$	even	17568.4819	0.0005		62
$3d^6(^5D)4s$	a^6D	1/2	even	17637.1570	0.0005		45
$3d^5(^6S)4s4p(^3P)$	z^8P	5/2	odd	18402.4843	0.0006		23
$3d^5(^6S)4s4p(^3P)$	z^8P	7/2	odd	18531.6651	0.0006		26
$3d^5(^6S)4s4p(^3P)$	z^8P	9/2	odd	18705.3600	0.0007		23
$3d^6(^5D)4s$	a^4D	$\frac{7}{2}$	even	23296.6821	0.0007		67
•••		·					
$3d^5(^2G)4s4p(^3P)$	u^2G	9/2	odd	68285.741	0.015		5
$3d^5(^2G)4s4p(^3P)$	u^2G	7/2	odd	68338.978	0.014		3
$3d^5(^4G)4s5s$	4G	$^{11}/_{2}$	even	68693.082	0.003		4
$3d^5(^4G)4s5s$	4G	9/2	even	68716.3459	0.0023		5
$3d^6(^1I)4p$	z^2K	$^{15}/_{2}$	odd	68797.703	0.013		1
$3d^6(^1I)4p$	z^2K	13/2	odd	68842.387	0.025		3
$3d^5(^2I)4s4p$	x^2I	$^{13}/_{2}$	odd	69560.811	0.01		2
$3d^5(^2I)4s4p$	x^2I	$11/_{2}$	odd	69629.671	0.018		3
$3d^6(^1I)4p$	v^2H	9/2	odd	69663.163	0.011		7
$3d^6(^1I)4p$	v^2H	$^{11}/_{2}$	odd	69722.908	0.006		7

Note. The columns are: (1-3) The configuration, term and J-value of the energy level. (4) The energy level value. (5) Energy level value uncertainty. (6) Flag: N = new level, A = anomalous hyperfine structure. (7) Number of lines contributing to the energy level optimisation. (This table is available in its entirety in machine-readable form)

the $3d^6(^3H)4p$ subconfiguration. These levels are not confirmed in our work and are therefore omitted from Table 5.

5.2.2. The $3d^6(^5D)6p$ subconfiguration

The only $3d^66p$ level listed in S&C is $3d^6(^5D)6p$ at 67890.00 cm⁻¹, but it was given neither a term nor J value in their compilation. No lines to this level were present in our spectra and therefore it was not confirmed in our analysis.

5.3. The Even Levels of the Doubly Excited System 5.3.1. Levels of the 3d⁵4s² configuration

The two electrons in the $3d^54s^2$ configuration mean that the 4s subshell is closed and so the term structure of the configuration is based on the grandparent terms of $3d^5$. we have found $3d^54s^2$ levels for the first five parent terms: $3d^5(^6S)4s^2$, (a^4G) , (a^4P) , (a^4D) and (a^2I) and these are all complete and revised in our work. No spectral lines from $3d^54s^2$ levels of the remaining parent terms were found.

5.3.2. Levels of the $3d^54s(^7S)ns$ and $3d^54s(^5S)5s$ subconfigurations

As discussed in Section 4, the $3d^5(^6S)$ grandparent term in Mn I is described using three separate term labels, with levels beyond 4s4p being assigned as $3d^54s(^7S)n'l'$ or $3d^54s(^5S)n'l'$. All of the ns levels for these subconfigurations listed in S&C have been confirmed and optimised in our analysis. The $3d^54s(^5S)5s$ subconfiguration is complete, but no further levels of the $3d^54s(^5S)ns$ subconfigurations have been found. The $3d^54s(^5S)5s$, 6s and 7s subconfigurations are also complete, with our new level for $3d^54s(^7S)7s$ $^8S_{7/2}$ at 54181.0432 cm $^{-1}$. For the $3d^54s(^5S)8s$ subconfiguration, we could only confirm the single level $g^8S_{7/2}$, with the $^6S_{5/2}$ level remaining unknown.

5.3.3. Levels of the $3d^54s(^7S)$ nd and $3d^54s(^5S)$ 5d subconfigurations

The $3d^54s(^5S)5d$ g^6D term is complete with all 5 levels newly optimised. The remaining 4 levels of the 4D term were not found in S&C or in our analysis. Both the $3d^54s(^7S)4d$ and $3d^54s(^7S)5d$ subconfigurations are fully complete, with ten levels found and optimised for each. The $3d^54s(^7S)6d$ subconfiguration is nearly complete, with only the two lowest-J levels of the g^8D term unknown.

The three lowest-J levels of the $3d^54s(^7S)5d$ f^8D term $(f^8D_{^3/2}, f^8D_{^5/2}$ and $f^8D_{^7/2})$ were unresolved in the previous work of S&C with 52702.48 cm⁻¹ given as the energy value for all three levels. This collective value had

relied on low resolution grating spectra recorded in the UV and had been determined from a blended transition to $3d^5(^6S)4s4p(^3P)$ $z^8P_{^5/2}$ identified at 34300.02 cm⁻¹. This transition is labelled as "wide and hazy" in M. A. Catalán et al. (1964) which was attributed to unresolved hyperfine structure. With the high resolution of FTS and the new IR FT spectra, strong, resolved transitions to these levels mean these have now been fully resolved. Positive identifications were also made with strong IR lines to $(^7S)5p$ levels, further securing the f^8D levels.

The five $3d^54s(^7S)7d$ h^8D_J levels were not resolved in S&C with 56801.4 cm⁻¹ being given as a collective energy. M. A. Catalán et al. (1964) had identified 4 transitions in the visible to secure these levels, but these lines were weak (intensity in Catalán of 1 and 5) and were labelled as hazy, probably indicating significant HFS which made them unsuitable for the determination of individual energy levels. These lines are resolved in our FTS spectra and enabled the establishment of four separate h^8D_J energy levels, resolved into J=11/2, 9/2, 7/2 and 5/2. Lines to the J=3/2 level were not observed in our new spectra and therefore an energy for this level was not determined.

5.4. The Odd Levels of the Doubly Excited System 5.4.1. Levels of the $3d^5(^2L)4s4p$ and $3d^5(^4L)4s4p$ subconfigurations

In total, 38 out of 43 4s4p levels belonging to doublet grandparent $3d^5(^2L)$ subconfigurations and 76 out of 86 levels belonging to quartet grandparent $3d^5(^4L)$ subconfigurations listed in S&C have been confirmed and optimised. Levels for subconfigurations of the highest doublet grandparent terms, $(b^2F), (a^2S), (b^2D)$ and (b^2G) remain unknown with no transitions to these levels observed.

The $3d^5(^4D)4s4p^{-4}F$ term is now complete following the redesignation of the levels 55405.1456 cm⁻¹ and 55368.6389 cm⁻¹ as $^4F_{5/2}$ and $^4F_{3/2}$ respectively.

5.4.2. Levels of the $3d^5(^6S)4s4p$, $3d^54s(^7S)np$ and $3d^54s(^5S)np$ subconfigurations

The $3d^5(^6S)4s4p$ subconfiguration is complete with 12 levels confirmed and optimised.

All of the $3d^54s(^5S)5p$ levels listed in S&C have also been confirmed. We were only able to determine one level for higher subconfigurations, $3d^54s(^5S)7p^{-6}P_{5/2}$, which was listed without a J-value in S&C, but which we were able to determine to be J=5/2.

The same situation is true for the $3d^54s(^7S)np$ subconfigurations with all levels confirmed for the lower lying subconfigurations of $3d^54s(^7S)5p$ and $3d^54s(^7S)6p$. We were unable to determine values for two 7p levels, $3d^54s(^7S)7p$ $^8P_{7/2}$ and $^8P_{5/2}$, and one 8p level, $3d^54s(^7S)8p$ $^8P_{^7/2}$. As discussed in Section 4, high order np configurations were not populated in our hollow cathode sources and therefore no spectral lines for transitions to subconfigurations above $3d^54s(^7S)8p$ were observed in our spectra.

5.4.3. Levels of the $3d^54s(^7S)nf$ subconfigurations

Five levels each of the w^6F and z^8F terms of the $3d^54s(^7S)4f$ subconfiguration have been found. The level $3d^54s(^7S)4f$ $w^6F_{^{1/2}}$, also not listed in S&C, was unable to be confirmed from lines in our spectra. In S&C, all the levels of the $3d^54s(^7S)4f$ z^8F term were given the energy 52974.50 cm⁻¹, but again due to the high resolution of our FT spectra, we have resolved the 5 highest-J levels and have been able to determine distinct level values for each. The two remaining, lowest-J levels of z^8F_J could not be found as their transitions are predicted to be weak.

Following our analysis, the term values of the $3d^54s(^7S)5f$ subconfigurations have been interchanged as the transitions observed in our FT and grating spectra matched far better with these exchanged term values. In addition, two levels designated $3d^54s(^7S)5f$ $v^6F_{11/2}$ and $v^6F_{9/2}$ in S&C (now redesignated $y^8F_{11/2}$ and $y^8F_{9/2}$ respectively) at 55499.09 cm⁻¹ have been resolved into two separate levels at 55499.709 cm⁻¹ and 55499.757 cm⁻¹.

S&C list levels in the $3d^54s(^7S)6f$ and 7f subconfigurations, but we were unable to confirm these levels as many high-lying levels were not populated in our hollow cathode sources and no spectral lines associated with them were present in our spectra.

5.4.4. Levels of the $3d^54p^2$ subconfiguration

Only three levels, $e^8P_{9/2}$, $e^8P_{7/2}$ and $e^8P_{5/2}$, of the $3d^54p^2$ subconfiguration, also listed in S&C, were found and optimised in our analysis.

5.5. Anomalous hyperfine structure

During the course of our analysis we noted that the hyperfine levels of several terms could not be fitted due to the dominance of off-diagonal hyperfine interactions. In normal cases, HFS is described using the diagonal interaction constants A and B, which assume that the total

angular momentum quantum number J is a good quantum number and that mixing between fine structure levels is negligible (M. Ding & J. C. Pickering 2020). However, the z^8F , f^8D , x^6D and w^6F terms exhibit strong hyperfine interactions, whilst the fine structure splitting between individual levels is unusually small. This combination leads to significant mixing between hyperfine levels derived from different fine structure components, rendering the diagonal approximation invalid and introducing large intensity redistributions among the component lines (M. Andersson et al. 2015). As a result, J loses its physical meaning, and the energy shifts and line intensities cannot be accurately described using standard hyperfine constants. Resolving these transitions would require extensive theoretical calculations accounting for the full off-diagonal interaction matrix for each transition which are beyond the scope of the present work. Levels which are potentially affected by anomalous hyperfine interaction have been highlighted in Table 5 with "A", to indicate the breakdown of the conventional hyperfine description and highlight that care should be taken when using these levels to determine Ritz wavelengths for transitions.

5.6. Summary of the Revision of Known Energy Level Values

In total, 384 of the 453 energy levels given in S&C (excluding Rydberg series levels) have been revised and optimised as a result of this analysis. The energy differences between our new values and those of S&C are shown in Figure 7. Error bars show the uncertainties of the energy levels from this analysis (in black) and from S&C's analysis of previously published levels (in red). The substantial reduction in uncertainty from the present analysis can be seen. Energy levels with the highest precision are typically those belonging to the quartet and sextet terms, due to their strong LS-allowed transitions to the ground state. Levels which were optimised exclusively using grating lines may have uncertainties exceeding 0.02 cm⁻¹ due to the much higher wavelength uncertainties compared to FTS measurements. In addition, the level designations of 52 levels have been revised following our analysis. These changes to energy level labels are detailed in Table 6.

 ${\bf Table~6.~Mn~I~Energy~Level~Label~Redesignations}$

Energy	Previous Label	New Label
(cm^{-1})	(J. Sugar & C. Corliss 1985)	(this work)
55368.6389	$3d^54s(^5S)5p \ w^4P_{3/2}$	$3d^5(^4D)4s4p^{-4}F_{3/2}$
55405.1456	$3d^54s(^5S)5p\ w^4P_{5/2}$	$3d^5(^4D)4s4p^{-4}F_{5/2}$
55495.185	$3d^54s(^7S)5f\ v^6F_{5/2}$	$3d^54s(^7S)5f\ y^8F_{5/2}$
55495.895	$3d^54s(^7S)5f\ v^6F_{7/2}$	$3d^54s(^7S)5f\ y^8F_{7/2}$
55495.933	$3d^54s(^7S)5f\ v^6F_{9/2}$	$3d^54s(^7S)5f\ y^8F_{9/2}$
55495.997	$3d^54s(^7S)5f\ v^6F_{11/2}$	$3d^54s(^7S)5f\ y^8F_{11/2}$
55499.709	$3d^54s(^7S)5f\ y^8F_{11/2}$	$3d^54s(^7S)5f\ v^6F_{11/2}$
55499.757	$3d^54s(^7S)5f\ y^8F_{9/2}$	$3d^54s(^7S)5f\ v^6F_{9/2}$
55499.764	$3d^54s(^7S)5f\ y^8F_{7/2}$	$3d^54s(^7S)5f\ v^6F_{7/2}$
55499.778	$3d^54s(^7S)5f\ y^8F_{5/2}$	$3d^54s(^7S)5f\ v^6F_{5/2}$
55499.85	$3d^54s(^7S)5f\ y^8F_{3/2}$	$3d^54s(^7S)5f\ v^6F_{3/2}$
56462.2247	$e^4 D_{7/2}$	$3d^6(^5D)5s\ e^4D_{7/2}$
56562.1994	$e^4 D_{5/2}$	$3d^6(^5D)5s\ e^4D_{5/2}$
56617.4657	$e^4 D_{3/2}$	$3d^6(^5D)5s\ e^4D_{3/2}$
57305.6987	$3d^6(^5D)5s\ f^4D_{7/2}$	$3d^64s(^5S)4p^{-4}D_{7/2}$
57486.1186	$3d^6(^5D)5s\ f^4D_{5/2}$	$3d^64s(^5S)4p^{-4}D_{5/2}$
57621.968	$3d^6(^5D)5s\ f^4D_{3/2}$	$3d^64s(^5S)4p^{-4}D_{3/2}$
57706.281	$3d^6(^5D)5s f^4D_{1/2}$	$3d^64s(^5S)4p^{-4}D_{1/2}$
59989.811	$3d^6(a^3P)4p^{-4}D_{3/2}$	$3d^6(a^3P)4p \ w^4D_{3/2}$
60141.928	$3d^6(a^3P)4p^{-4}D_{1/2}$	$3d^6(a^3P)4p \ w^4D_{1/2}$
60395.523	$3d^6(a^3P)4p^{-2}D_{3/2}$	$3d^6(a^3P)4p\ z^2D_{3/2}$
61469.12	$3d^6(^3G)4p^{-4}G_{11/2}$	$3d^6(^3G)4p \ w^4G_{11/2}$
62670.96	$3d^5(^4F)4s4p(^3P)^{-6}D_{9/2}$	$3d^5(^4F)4s4p(^3P) \ w^6D_{9/2}$
63139.604	$3d^5(^4G)4s4p(^1P)^{-4}F_{5/2}$	$3d^5(a^2F)4s4p^4G_{5/2}$
63288.7081	$3d^6(^3G)4p^{-2}H_{11/2}$	$3d^6(^3G)4p \ z^2H_{^{11/2}}$
63288.714	$3d^5(^4G)4s4p(^1P)_{7/2}$	$3d^5(a^2F)4s4p^4G_{7/2}$
63548.4622	$3d^6(^3G)4p^{-2}H_{9/2}$	$3d^6(^3G)4p\ z^2H_{9/2}$
64051.7993	$3d^5(^2I)4s4p(^3P)^{-2}I_{11/2}$	$3d^5(^2I)4s4p^{-2}I_{13/2}$
64055.271	9/2	$3d^5(^2I)4s4p^{-2}I_{11/2}$
64585.331	$3d^5(a^2F)4s4p(^3P)^{-4}F_{9/2}$	$3d^5(a^2F)4s4p \ x^2G_{9/2}$
64649.082	$3d^5(a^2F)4s4p(^3P) \ w^2G_{7/2}$	$3d^5(a^2F)4s4p \ x^2G_{7/2}$
64806.961	$3d^54s(^5S)7p^{-6}P$	$3d^54s(^5S)7p^{-6}P_{5/2}$
65305.299	7/2	$3d^5(a^2F)4s4p(^3P) \ w^2G_{7/2}$
65617.305	$3d^6(^3G)4p_{7/2}$	$3d^6(^3G)4p\ v^2F_{7/2}$
65768.744	$3d^6(^3G)4p_{9/2}$	$3d^6(^3G)4p^{-2}G_{9/2}$
65873.286	$3d^6(^3H)4p_{5/2}$	$3d^6(^3H)4p \ v^4G_{5/2}$
65876.268	$3d^6(^3H)4p_{7/2}$	$3d^6(^3H)4p \ v^4G_{7/2}$
65961.777	$3d^5(^4P)4s4p(^1P)_{3/2}$	$3d^5(^2D)4s4p \ w^2D_{3/2}$
66395.077	$3d^5(^4F)4s4p(^3P)_{5/2}$	$3d^5(^4F)4s4p(^3P) \ u^4G_{5/2}$

Table 6 continued

Table 6 (continued)

Energy	Previous Label	New Label
(cm^{-1})	(J. Sugar & C. Corliss 1985)	(this work)
66454.18	$3d^5(^4F)4s4p(^3P)_{7/2}$	$3d^5(^4F)4s4p(^3P) \ u^4G_{7/2}$
67504.945	$3d^6(^1I)4p \ w^2H_{^{11/2}}$	$3d^6(^1G)4p \ w^2H_{11/2}$
67576.81	$3d^6(^1I)4p \ w^2H_{9/2}$	$3d^6(^1G)4p \ w^2H_{9/2}$
68285.741	$3d^5(^4F)4s4p(^3P)^{-4}F_{9/2}$	$3d^5(^2G)4s4p(^3P) \ u^2G_{9/2}$
68338.978	$3d^5(^4F)4s4p(^3P)^{-4}F_{7/2}$	$3d^5(^2G)4s4p(^3P) \ u^2G_{7/2}$
68693.082	$3d^54s(^5G)5s\ f^4G_{11/2}$	$3d^5(^4G)4s5s\ ^4G_{11/2}$
68716.3459	$3d^54s(^5G)5s\ f^4G_{9/2}$	$3d^5(^4G)4s5s\ ^4G_{9/2}$
68797.703	$z^2 K_{15/2}$	$3d^6(^1I)4p\ z^2K_{15/2}$
68842.387	$z^2 K_{13/2}$	$3d^6(^1I)4p\ z^2K_{13/2}$
69560.811	$x^2I_{13/2}$	$3d^5(^2I)4s4p \ x^2I_{13/2}$
69629.671	$x^2I_{11/2}$	$3d^5(^2I)4s4p \ x^2I_{11/2}$
69663.163	$v^2 H_{9/2}$	$3d^6(^1I)4p\ v^2H_{9/2}$
69722.908	$v^2 H_{11/2}$	$3d^6(^1I)4p \ v^2H_{^{11/2}}$

6. IDENTIFICATION OF NEW ENERGY LEVELS

Following the revision of known energy levels, unclassified lines remaining in our linelist were used to search for new energy levels. To identify potential new energy levels, we combined the wavenumbers of unassigned spectral lines with our optimised energy level dataset. The resulting values were then examined for clusters of transitions falling within a given wavenumber tolerance, typically within ± 0.05 cm⁻¹, that might signify the presence of new levels. Theoretical calculations provided useful guides for approximate level energies and predicted transition strengths to help determine identifications of newly found levels. In particular, the work of the late R. L. Kurucz (2016) was invaluable in our search for new levels. In total, 18 new energy levels of Mn I, reported here for the first time, have been identified and optimised as a result of our analysis. Details of the determination of these new levels are given below.

6.1. New levels of the $3d^54s(^7S)nl$ subconfigurations 6.1.1. The $3d^54s(^7S)6p$ $^8P_{9/2}$ level

This level was the only level missing from the $4s(^7S)6p$ 8P term in S&C. Our new IR FT measurements, lines to 6s and 4d levels of the same parent term enabled the optimisation of this level. Three FT lines and one grating line have now been newly classified as transitions from the $3d^54s(^7S)6p$ $^8P_{9/2}$ level at 52506.8046 cm⁻¹.

6.1.2. The
$$3d^54s(^7S)7s$$
 $^8S_{7/2}$ level

This is the only level within the $3d^54s(^7S)7s$ 8S term that we were able to determine, as the remaining levels have lines predicted to be very weak and which were not observed in our spectra. The new level at 54181.0432 cm⁻¹ was identified using FT lines in the IR to levels of $4s(^7S)5p$ and in the visible to levels of $(^6S)4s4p(^3P)$. Six new lines have now been classified as transitions from this level.

6.1.3. The
$$3d^54s(^7S)5f$$
 $y^8F_{13/2}$ level

A level with this designation had previously been reported in S&C at 55498.5 cm⁻¹. However, following our analysis it was determined that the y^8F and v^6F terms should be swapped and that this level energy should be discarded. Our new energy value for $y^8F_{13/2}$ is at 55496.0799 cm⁻¹, and there are reliable FT transitions in the IR linking to $3d^54s(^7S)4d$ and 5d levels, securing this level well in the optimised fit.

6.1.4. The
$$3d^54s(^7S)7p^6P_{3/2}$$
 level

A new FT transition in the IR, at 6082.3287 cm⁻¹, enabled the identification of this new $3d^54s(^7S)7p$ $^6P_{3/2}$ level, and a grating line in the visible ensured its optimised fit at 55497.7276 cm⁻¹. This new level completes the $3d^54s(^7S)7p$ 6P term.

6.2. The
$$3d^6(^5D)5s\ e^4D_{^{9/2}}\ level$$

The previous level in S&C with the designation $3d^6(^5D)5s\ e^4D_{^9/2}$ at 56601.63 cm⁻¹ has now been discarded following our analysis. Strong transitions in the visible to levels of the $(^6S)4s4p(^3P)$ subconfiguration

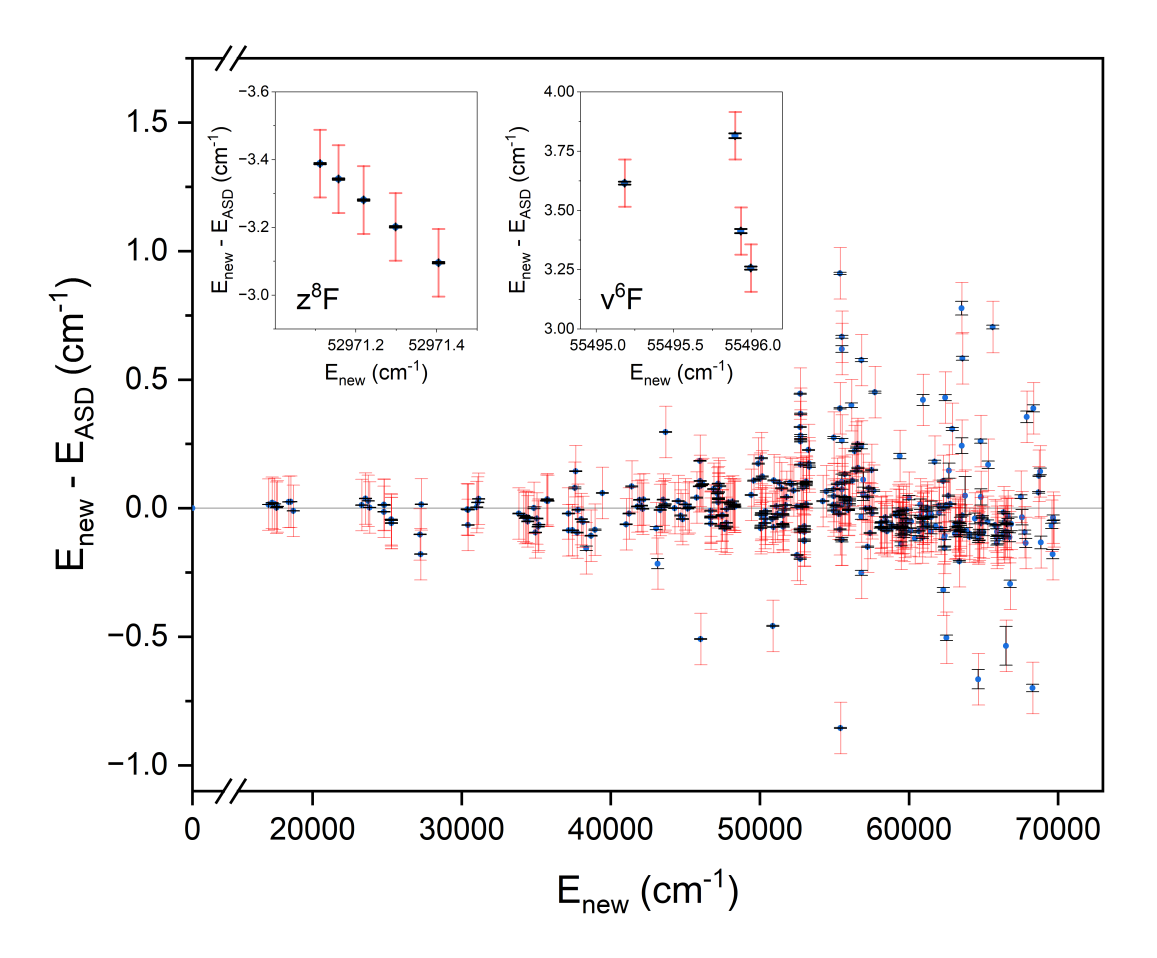


Figure 7. Comparison of our revised Mn I energy levels and the previously published values of J. Sugar & C. Corliss (1985). The uncertainties of S&C are shown in red and our uncertainties are in black. The levels of the z^8F and v^6F terms have now been resolved and shifted considerably in our new analysis (note the different axes scales). These levels are given in inset plots to ensure that the main plot scale provides sufficient detail of the other levels.

enabled the identification of a new level at 56617.4657 cm⁻¹, and these lines fitted very clearly with theoretical line strengths. In total, five FT and one grating line have been classified for the first time.

6.3. The
$$3d^6(^3H)4p \ z^4I_{11/2} \ level$$

Again, this is a designation that had previously been identified in S&C, but whose level has now been discarded following our analysis. A new energy level at 58827.4893 cm⁻¹ has determined for this $3d^6(^3H)4p$ $z^4I_{11/2}$ designation. The strong FT line to $3d^6(^3H)4s$ $a^4H_{9/2}$ fits very clearly with the multiplet pattern of transitions and relative line intensities of the other $3d^6(^3H)4p$ z^4I_J levels, providing certainty about the identification of this level.

6.4. New levels of the quartet parent term $3d^5(^4L)4s4p$ subconfigurations

The majority of the new energy levels determined in this work are odd levels of the 4s4p subconfigurations with quartet parent terms, (^4L) . These are:

• $({}^{4}G)4s4p$: ${}^{2}H_{11/2}$, ${}^{2}H_{9/2}$, ${}^{2}F_{7/2}$ and ${}^{2}F_{5/2}$

• $(^4P)4s4p$: $^2P_{3/2}$, $^2P_{1/2}$ and $^2D_{3/2}$

 \bullet (^4D)4s4p: ^4F_{9/2}, ^4F_{7/2} and ^2F_{5/2}

• $({}^4G)4s4p$: ${}^4G_{7/2}$ and ${}^2G_{9/2}$

It is surprising that these levels were not identified by M. A. Catalán et al. (1964) as their transitions are strong and in the visible spectral region where Catalán had spectra. It is therefore likely that these levels were weakly populated in the sources used by Catalán and the resultant lines in their spectra were very weak. Regardless, these levels were well populated in our sources, and our FT and grating data enabled excellent fits for these new levels to well-secured lower energy levels, resulting in the establishment of 12 new levels and the new classification of 103 spectral lines.

6.5. The
$$(^{2}I)4s4p^{-4}K_{^{11/2}}$$
 level

The new $(^2I)4s4p$ $^4K_{^{11}/^2}$ level is now found and is secured by FT lines in the visible to the singly excited

system through transitions to levels of $(^4H)4s$, and to the doubly excited system through transitions to levels of $3d^54s^2$. Five FT lines have been classified for the first time due to the determination of this level.

7. SUMMARY

New atomic data for Mn I are urgently needed for the analysis of astrophysical spectra. Previous atomic data for energy levels and wavelength of Mn I were based on measurements taken over 60 years ago, pre-dating the development of high-resolution FT spectroscopy. These data are now of insufficient accuracy for modern astrophysical spectral analyses.

Following an extensive term analysis of the spectrum of Mn I, measured using high-resolution FT and grating spectroscopy, 384 previously reported energy levels have been revised with a significant improvement in accuracy - an improvement in uncertainty of at least an order-of-magnitude. 18 completely new Mn I energy levels have also been found and optimised for the first time. The classified linelist for Mn I now contains 2186 lines, with 1642 FT and 289 newly-measured grating lines.

This work represents the most accurate Mn I wavelength and energy level values available to date. These

data will enable far more accurate and reliable analyses of Mn I transition lines in astrophysical spectra.

ACKNOWLEDGMENTS

CPC and JCP thank the STFC of the UK for their support through the grants ST/K001051/1, ST/S000372/1, ST/W000989/1 and UKRI1188. JCP thanks the Royal Society for URF support during the 2001 spectral measurements. In addition, RBW expresses his gratitude to Sveneric Johansson and Hampus Nilsson for their advice and guidance with term analysis, and gratefully acknowledges the Valery Myerscough Prize for funding his research visit to the Lund Observatory, Sweden. MTB thanks the Ministerio de Ciencia, Innovación y Universidades of the Spanish Government for her Beatriz Galindo Fellowship and acknowledges funding from MICIU/AEI /10.13039/501100011033 and by FEDER (UE) under project PID2021-127786NA-100.

JCP thanks the late Bob Kurucz for his extensive theoretical calculations that have aided spectrum analysis research at Imperial over the past 35 years.

REFERENCES

Andersson, M., Grumer, J., Ryde, N., et al. 2015, Astrophysical Journal Supplement Series, 216, 2, doi: 10.1088/0067-0049/216/1/2

Bergemann, M., Gallagher, A. J., Eitner, P., et al. 2019, A&A, 631, A80, doi: 10.1051/0004-6361/201935811

Blackwell-Whitehead, R., Pickering, J., Pearse, O., & Nave, G. 2005, ApJS, 157, 402, doi: 10.1086/427924

Blackwell-Whitehead, R. J. 2003, PhD thesis, Imperial College, University of London

Catalán, M. A. 1923, RSPTA, 223, 127, doi: https://doi.org/10.1098/rsta.1923.0004

Catalán, M. A., Meggers, W. F., & García-Riquelme, O. 1964, J. Res. Natl. Bur. Stand. A Phys. Chem., 68A, 9

Clear, C. P., Pickering, J. C., Nave, G., Uylings, P., & Raassen, T. 2022, ApJS, 261, 35,

doi: 10.3847/1538-4365/ac7f9b

Clear, C. P., Pickering, J. C., Nave, G., Uylings, P., & Raassen, T. 2023, ApJS, 269, 36, doi: 10.3847/1538-4365/ad04d4

Ding, M., & Pickering, J. C. 2020, ApJS, 251, 24, doi: 10.3847/1538-4365/abbdf8

García-Riquelme, O. 1949, An. R. Soc. Esp. Fis. Quim., 45A, 435–448

Ginter, M. L., & Brown, C. M. 1978, JOSA, 68, 1541

Kling, R., & Griesmann, U. 2000, ApJ, 531, 1173, doi: 10.1086/308490

Kramida, A., & Nave, G. 2006, EPJD, 39, 331, doi: 10.1140/epjd/e2006-00121-4

Kramida, A., Nave, G., & Reader, J. 2017, Atoms, 5, doi: 10.3390/atoms5010009

Kramida, A., Yu. Ralchenko, Reader, J., & and NIST ASD Team. 2019, NIST Atomic Spectra Database (ver. 5.7.1), National Institute of Standards and Technology, Gaithersburg, MD. doi: 10.18434/T4W30F

Kramida, A. E. 2011, CoPhC, 182, 419, doi: 10.1016/j.cpc.2010.09.019

doi: 10.1016/j.cpc.2010.09.019

Kurucz, R. L. 2016, Atomic Level Data for Mn I: files created on 15-Dec-2016,

http://kurucz.harvard.edu/atoms/2500/

Learner, R. C. M., & Thorne, A. P. 1988, JOSA B, 5, 2045, doi: 10.1364/JOSAB.5.002045

Liggins, F. 2017, PhD thesis, Imperial College, University of London, doi: https://doi.org/10.25560/59134

Liggins, F. S., Pickering, J. C., Nave, G., Ward, J. W., & Tchang-Brillet, W. L. 2021, ApJS, 252, 10

Litzén, U., Brault, J. W., & Thorne, A. P. 1993, PhyS, 47, 628, doi: 10.1088/0031-8949/47/5/004

- McLennan, J. C., & McLay, A. 1926, Trans. Roy. Soc. Can., 20, 89
- Moore, C. E. 1945, Contributions from the Princeton University Observatory, 20, 1
- Nave, G., Griesmann, U., Brault, J. W., & Abrams, M. 2015, Xgremlin: Interferograms and spectra from Fourier transform spectrometers analysis, doi: 2015ascl.soft11004N
- Nave, G., Sansonetti, C. J., & Griesmann, U. 1997, Fourier Transform Spectroscopy (1997), FMC.3, doi: 10.1364/FTS.1997.FMC.3
- Peck, E. R., & Reeder, K. 1972, JOSA, 62, 958, doi: 10.1364/JOSA.62.000958
- Pulliam, B. V. 1979, M.s. thesis, Purdue University, West Lafayette, Indiana
- Saloman, E. B., & Sansonetti, C. J. 2004, J. Phys. Chem. Ref. Data, 33, 1113, doi: 10.1063/1.1797771

- Sansonetti, J. E., Reader, J., Sansonetti, C. J., & Acquista, N. 1992, J. Res. Natl. Inst. Stand. Technol., 97, 1, doi: 10.6028/jres.097.002
- Sugar, J., & Corliss, C. 1985, J. Phys. Chem. Ref. Data, 14Taklif, A. G. 1990, PhyS, 42, 69
- Thorne, A. 1996, PhyS, T65, 31, doi: 10.1088/0031-8949/1996/T65/004
- Thorne, A. P., Harris, C. J., Wynne-Jones, I., Learner, R.
 C. M., & Cox, G. 1987, J. Phys. E: Sci. Instr., 20, 54,
 doi: 10.1088/0022-3735/20/1/010
- Whaling, W., Anderson, W., Carle, M., Brault, J., & Zarem, H. 1995, JQSRT, 53, 1, doi: https://doi.org/10.1016/0022-4073(94)00102-D
- Whaling, W., Anderson, W. H. C., Carle, M. T., Brault, J. W., & Zarem, H. A. 2002, J. Res. Natl. Inst. Stand. Technol., 107, 149, doi: 10.6028/jres.10714